DESIGN AND MODELLING OF A HYBRID PRESSURE REGULATOR

A THESIS SUBMITTED TO
THE GRADUATE SCHOOL OF NATURAL AND APPLIED SCIENCES
OF
MIDDLE EAST TECHNICAL UNIVERSITY

BY

MEHMET GÖKALP GÜRFİDAN

IN PARTIAL FULFILLMENT OF THE REQUIREMENTS
FOR
THE DEGREE OF MASTER OF SCIENCE
IN
MECHANICAL ENGINEERING

SEPTEMBER 2022

Approval of the thesis:

DESIGN AND MODELLING OF A HYBRID PRESSURE REGULATOR

submitted by **MEHMET GÖKALP GÜRFİDAN** in partial fulfillment of the requirements for the degree of **Master of Science** i**n Mechanical Engineering, Middle East Technical University** by,

Prof. Dr. Halil Kalıpçılar
Dean, Graduate School of **Natural and Applied Sciences** _____

Prof. Dr. M. A. Sahir Arıkan
Head of the Department, **Mechanical Engineering** _____

Prof. Dr. Yiğit Yazıcıoğlu
Supervisor, **Mechanical Engineering, METU** _____

Examining Committee Members:

Prof. Dr. Mehmet Metin Yavuz
Mechanical Engineering Dept., METU _____

Prof. Dr. Yiğit Yazıcıoğlu
Mechanical Engineering Dept., METU _____

Assist. Prof. Dr. Özgür Uğraş Baran
Mechanical Engineering Dept., METU _____

Assist. Prof. Dr. Hakan Çalışkan
Mechanical Engineering Dept., METU _____

Assist. Prof. Dr. Emir Kutluay
Mechanical Engineering Dept., Hacettepe University _____

Date: 14.09.2022

I hereby declare that all information in this document has been obtained and presented in accordance with academic rules and ethical conduct. I also declare that, as required by these rules and conduct, I have fully cited and referenced all material and results that are not original to this work.

Name Last name : Mehmet Gökalp Gürfidan

Signature :

ABSTRACT

DESIGN AND MODELLING OF A HYBRID PRESSURE REGULATOR

Gürfidan, Mehmet Gökalp
Master of Science, Mechanical Engineering
Supervisor : Prof. Dr. Yiğit Yazıcıoğlu

September 2022, 92 pages

Pressure regulator is used for regulating high upstream pressure to required low downstream pressure. It is especially an important component for space applications where an accurate pressure control is vital, and failure to do so can cause mission failure. In this thesis a novel pressure regulator design is modeled that eliminates the inherent steady state error of purely mechanical pressure regulator by introducing cascaded electromechanical actuator. Dynamic components of the proposed hybrid pressure regulator are explained and mathematically modeled. Three system models are derived, namely nonlinear system model, simplified nonlinear model and linearized model. PID controller is designed for the actuator. Finally, hybrid pressure regulator is simulated using Matlab-Simulink with different operation scenarios with and without fault injection, and results are compared with a traditional mechanical pressure regulator having same design parameters.

Keywords: Pressure Regulator, Nonlinear System Model, Controller Design

ÖZ

HİBRİT BASINÇ DÜZENLEYİCİ TASARIMI VE MODELLEMESİ

Gürfidan, Mehmet Gökalp
Yüksek Lisans, Makina Mühendisliği
Tez Yöneticisi: Prof. Dr. Yiğit Yazıcıoğlu

Eylül 2022, 92 sayfa

Basınç regülatörü, yüksek giriş basıncını, istenen çıkış basıncına düşürmek için kullanılır. Özellikle uzay uygulamalarında, hassas çıkış basınç kontrolü hayati önem taşır ve kontrolün sağlanamaması görev başarısızlığı ile sonuçlanabilmektedir. Bu tezde özgün basınç regülatörü tasarımı modellenmiştir. Özgün hibrit tasarımı ile, klasik mekanik basınç regülatörlerinin önüne geçilemeyen kalıcı çıkış basınç hatası, elektromekanik eyleyici ile kapatılabilmektedir. Önerilen hibrit basınç regülatörünün dinamik aksamları açıklanmış ve matematiksel olarak modellenmiştir. Doğrusal olmayan sistem modeli, basitleştirilmiş doğrusal olmayan sistem modeli ve doğrusallaştırılmış sistem modeli olmak üzere üç farklı sistem modeli türetilmiştir. Türetilen sistem modelleri kullanılarak, eyleyici için kontrolcü tasarlanmıştır. Son olarak, hibrit basınç regülatörü modellerinin Matlab-Simulink ortamında bilgisayar benzetimleri gerçekleştirilerek, farklı operasyon senaryoları için sonuçları karşılaştırılmıştır.

Anahtar Kelimeler: Basınç Regülatörü, Doğrusal Olmayan Sistem Modeli, Kontrolcü Tasarımı

To My Parents, Little Sibling

and

My Love Betül T. Gürfidan

ACKNOWLEDGMENTS

I would like to express my gratitude to my supervisor Prof. Dr. Yiğit YAZICIOĞLU. During preparation of the thesis, he gave me his support by helpful criticism, guidance, and patience.

I would like to extend my thanks to EKİNOKS-AG, for their generous support and guidance towards higher academical education. My special thanks to Dr. Erdinç N. YILDIZ, for his technical support that leads a way out whenever I am lost.

I want to send my thanks to all members of my family for believing and supporting me through this process. Thanks for being there all the time.

And finally, very special thanks to my beloved wife Betül Terzioğlu GÜRFİDAN, who supported me in every step of the way. I could not have finished this thesis without her endless support and motivation.

TABLE OF CONTENTS

LIST OF TABLES

TABLES

LIST OF FIGURES

FIGURES

LIST OF ABBREVIATIONS

ABBREVIATIONS

CV	Control Volume
DOF	Degree of Freedom
PID	Proportional-Integral-Derivative
PR	Pressure Regulator
VCA	Voice Coil Actuator

LIST OF SYMBOLS

SYMBOLS

$A_{piston,l}$	Piston lower side net area
$A_{piston,u}$	Piston upper side net area
$A_{poppet,b}$	Poppet bottom area
$A_{poppet,s}$	Poppet shoulder area
$A_{seat,l}$	Seat lower side projected area perpendicular to x-axis
$A_{seat,u}$	Seat upper side projected area perpendicular to x-axis
$C_{d,i}$	Discharge coefficient of inlet port
$C_{d,o}$	Discharge coefficient of outlet port
$C_{d,s}$	Discharge coefficient of sensing port
CV_{inlet}	Inlet control volume
CV_{outlet}	Outlet control volume
CV_{piston}	Piston control volume
d_1	Poppet seat diameter
$F_{actuation}$	Effective force of voice coil on the poppet-piston assembly
$F_{coul,piston}$	Piston seal coulomb friction
$F_{coul,poppet}$	Poppet seal coulomb friction
Fc_{vca}	Voice coil actuator force constant
F_{fric}	Total friction force
F_{sp1}	Spring1 force
F_{sp2}	Spring2 force
F_{vc}	Voice coil force
$G_{cl}(s)$	Closed loop transfer function
$G_{cont}(s)$	Control transfer function
$G_{iP}(s)$	Current to outlet pressure transfer function

$G_{red}(s)$	Reduced order transfer function
i_{vc}	Voice coil current
k_1	Spring1 stiffness
k_2	Sprign2 stiffness
K_d	Derivative controller gain
K_i	Integral controller gain
K_p	Proportional controller gain
K_u	Ultimate gain
$m_{actuation}$	Mass of actuator
m_{lever}	Mass of lever
m_{piston}	Mass of piston
m_{poppet}	Mass of poppet
m_{sp1}	Mass of spring1
m_{sp2}	Mass of spring2
$m_{springs}$	Total mass of springs
m_{vc}	Voice coil moving mass
$\dot{m}_{in}$	Mass flow rate into control volume
$\dot{m}_{inlet}$	Inlet port mass flow rate
$\dot{m}_{sensing}$	Sensing port mass flow rate
$\dot{m}_{out}$	Mass flow rate out of control volume
$\dot{m}_{outlet}$	Application mass flow rate demand
P_{amb}	Ambient pressure
P_{crit_ratio}	Pressure critical ratio for choked flow
P_{inlet}	Pressure of inlet control volume
P_{outlet}	Pressure of outlet control volume
P_{piston}	Pressure of piston control volume
R	Individual gas constant of helium
r_{lever}	Lever ratio
T_{inlet}	Temperature of inlet control volume

T_{outlet}	Temperature of outlet control volume
T_{piston}	Temperature of piston control volume
V_{inlet}	Volume of inlet control volume
V_{outlet}	Volume of outlet control volume
V_{piston}	Volume of piston control volume
$V_{piston,0}$	Initial volume of piston control volume
x_p	Position of the moving assembly
x_{design}	Position of the moving assembly at design point
β	Lever angle
$\delta_{sp1,pre}$	Precompression of spring1
$\delta_{sp2,pre}$	Precompression of spring2
θ	Seat angle
γ	Ratio of specific heats of helium

CHAPTER 1

INTRODUCTION

1.1 Aim of the Study

Pneumatic technology was first developed in the military field to realize the stable control of the space vehicle and the missile altitude [1]. As one of the main products of pneumatic technology, pressure regulators are utilized to regulate the working pressure for plants and machines. Critically, in aerospace propulsion systems, it is used to pressurize liquid propellant rocket tanks at specified pressure for obtaining the required propellant mass flow rate, or similarly to rapidly regulate the back pressure of an on/off solenoid valve in a cold gas thruster system.

Most commonly, pressure regulators are either purely mechanical devices or require electronical actuation to regulate the pressure. Especially, in aerospace applications purely mechanical pressure regulators are overwhelmingly preferred over electronical counter-parts since reliability demand is very high.

In this study, the model of a hybrid pressure regulator is developed. Challenge is to design a pressure regulator that can operate purely mechanical and capable of being coupled with an electronic actuation to enhance the regulation accuracy. Developed design is capable of reducing the inherent steady state error of purely mechanical pressure regulator also, it can keep regulating in case of power loss which makes it safer and more reliable than electronically actuated pressure regulators.

In this thesis, high fidelity nonlinear system dynamic model of a hybrid pressure regulator is formed. Nonlinear model is then simplified and linearized around an operation point to achieve a linearized plant model. A Proportional-Integral (PI)

controller for voice coil actuator is designed using linearized plant model. Finally, possible operation scenarios are defined and simulations for non-linear, simplified non-linear and linear hybrid pressure regulator models with and without control effort is run to observe the effect of voice coil actuation on pressure regulator performance.

1.2 Scope of the Thesis

In Chapter 1, the general information behind the working principle of a pressure regulator is given. Main components and their variations are introduced. Role of each component in a pressure regulator is explained.

In Chapter 2, the physical system is explained and modelled in detail. Firstly, generic governing equations that are used during modelling phase are introduced. Then, generic governing equations are employed for the specific modelling case. Simplifications are made to achieve simplified non-linear model. Lastly, simplified non-linear model is linearized around an operating condition to obtain linearized system model. then are introduced f The subcomponents of the system are interpreted, and non-linear mathematical model of the overall system is developed with necessary assumptions. Then, simple mechanism to increase the electronic actuation force is synthesized.

In chapter 3, operational envelope of the pressure regulator is defined, and parameters of the designed hybrid pressure regulator are listed together with other numerical values that are used during simulation. Transfer function between voice coil current and outlet pressure is derived and a PI controller is designed for the voice coil actuator.

In Chapter 4, various operational scenarios are defined. Simulation results of non-linear, simplified non-linear and linear model of the hybrid pressure regulator are compared with each other. Also, simulations are made with and without the

electronical actuation system to assess the performance of the proposed hybrid design over a traditional purely mechanical design.

In Chapter 5, conclusion and related future works are discussed.

1.3 Background and Basic Concepts

1.3.1 General Information about Pressure Regulators

Gas pressure regulators are devices that try to maintain constant output pressure regardless of the variations in inlet pressure and outlet flow [2]. They have both mechanical and electromechanical variations. They range from simple, single stage [3], [4] to more complex, multi stage [5], [6], however main operation principle remains the same. High pressure inlet gas flows through the orifice of the regulator which restricts the flow according to outlet pressure. As outlet pressure increases, poppet moves towards its closing position, reducing the orifice area and consequently flowrate through the regulator is decreased until the new equilibrium point is reached between flow through regulator and downstream flow demand. Similarly, as outlet pressure decreases, poppet moves away from its closing position, increasing the flow area and consequently flowrate through the regulator is increased. Thus, outlet pressure stabilizes at a new equilibrium point around its nominal set pressure. Variation between the equilibrium point and nominal set pressure depends on upstream pressure, upstream temperature, and downstream mass flow rate. The variation is referred as regulation accuracy.

1.3.2 Main Components of Pressure Regulators

There are three main components for a pressure regulator to operate as intended. Those components are loading element, sensing element and control element. In Figure 1.1, mentioned components for a mechanical pressure regulator are shown.

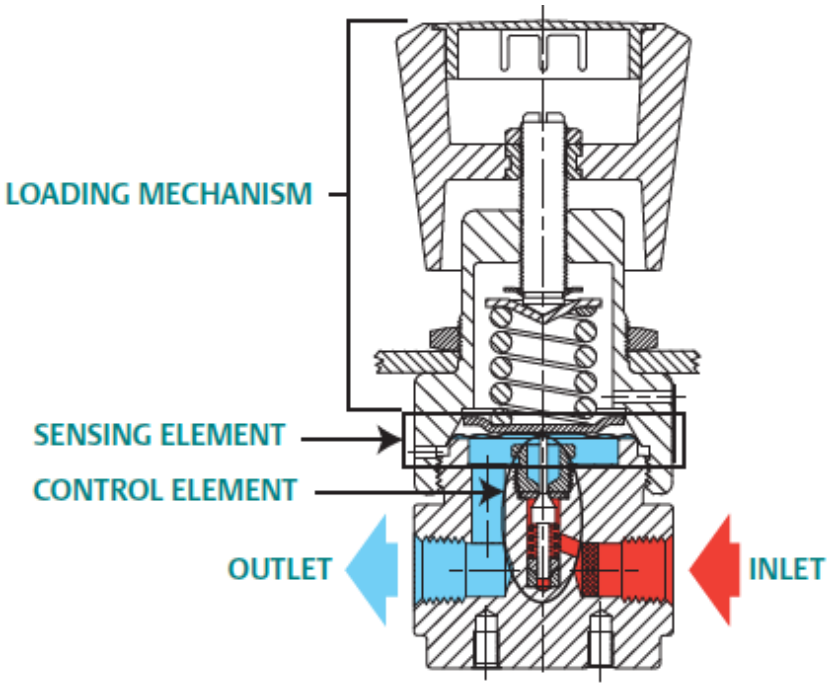

Figure 1.1. Generic Mechanical Pressure Regulator Crossection

Since pressure regulator is a control device, a closed loop block diagram can be drawn which is presented in Figure 1.2.

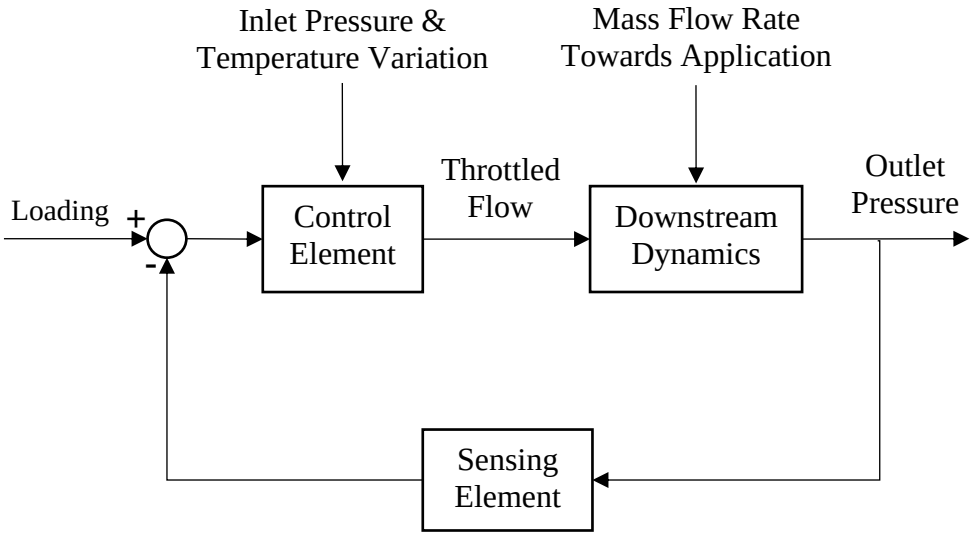

Figure 1.2. Block Diagram of Mechanical Pressure Regulator

Loading is generated by a loading mechanism, acts as a reference signal for the control loop. Sensing element senses the outlet pressure and creates feedback force against the reference force. Difference between reference and feedback force creates net force that drives control element. Control element regulates the opening of the regulator orifice, which creates throttled flow whose amount also depends on the inlet pressure and temperature. Flows into and out of downstream drives the downstream dynamics. Then, the pressure of the downstream is sensed by the sensing element and feedback control loop is completed.

1.3.2.1 **Loading Element**

A regulating point is required for any regulatory system. Loading element creates a reference for the regulation. Reference can be created in the form of force via loading mechanism, or it can be in the form of electrical signal.

Mechanical loading is used when the outlet pressure is sensed by a mechanical sensing element. It can be created via compressed spring or pressurized fluid. This type of loading creates a force which counteracts the force formed by the outlet pressure. Any difference between these forces creates a non-zero net force and actuates the system to a quasi-static condition.

Electronical loading is an electronical reference signal which can be compared with the signal obtained from pressure transmitter. Any difference between reference electronical signal and pressure transmitter signal results in a regulatory movement.

1.3.2.2 **Sensing Element**

Sensing element is used for closing the control loop with an information about the outlet pressure. It can be in the form of mechanical and electronical sensing.

Mechanical sensing can be accomplished by using piston or membrane. It creates an area on which outlet pressure creates a force. Force created by the outlet pressure on the sensing element can be used as feedback.

Pressure transmitter is used for electronical sensing. A sensor placed in outlet, feeds the control unit with a pressure information which is compared to reference signal.

1.3.2.3 **Control Element**

Control element controls the orifice area where the flow from inlet to outlet takes place. As the outlet pressure decreases control element moves away from its seating to increase the orifice area, conversely, as the outlet pressure increases control element moves towards its seating to decrease the orifice area up to a point where control element contacts with its seating and closes the orifice fully.

CHAPTER 2

SYSTEM MODELING

For a long time only accepted way to develop a pressure regulator type of device was by trial-and-error [7]. Most probable, this was the result of the inherent difficulties in the modelling of these regulators, due to the nonlinearities and coupling among the equations describing the dynamics of both the fluids and the mechanical parts. The main source of nonlinearities are the gas processes, the dry Coulomb friction acting on the poppet-command piston assembly, and the dependency of the free cross-flow area on the poppet location [8]. Tsai and Cassidy is one of the first paper that develops an analytical model for a pressure regulator [7]. In the paper, linear and non-linear models for a piston-poppet type mechanical pressure regulator were developed and transient and steady state response of those models were discussed. M. Avram, M. F. Tefănescu, A. Erban, A. Dobrovicescu, and B. Grămescu developed system model of an electronically actuated pressure regulator [9]. Thus, their model includes dynamics of the electronic feedback and actuation device. However, modelled pressure regulator requires electricity to be able to work. In the literature, there are numerous system models for mechanical pressure regulators [10],[11],[12] and electronical regulators [13][14][15]. There are little to no information regarding to system model for a hybrid pressure regulator which is the combination of mechanical pressure regulator that has a simple poppet-piston assembly, with an electronical feedback and actuation system. Motivation to develop such a design is to combine advantages of mechanical and electronical pressure regulators into one hybrid design. Design aims to achieve highly reliable, fast acting mechanical regulator characteristic together with high accuracy of an electronical regulator.

Pressure regulator is normally an open valve that has varying orifice area according to difference between reference force and sensed force created by the outlet pressure.

As long as the upstream pressure is higher than the downstream pressure and orifice area is non-zero there will be mass flow rate through the orifice. As the downstream pressure increases due to the mentioned mass flow rate, the force created by the downstream pressure on the piston increases which creates a net force on the single degree of freedom system. According to equation of motion, poppet moves towards to poppet seat and reduces the orifice area. This movement stops when the net force on the moving parts of the regulator is zero. Since the net force is highly dependent on the outlet pressure, in equilibrium point, outlet pressure stays constant. Hence, in the equilibrium point, mass flow rate through the pressure regulators orifice area and application flow rate demand is in balance and equal so that outlet pressure stays constant. In order to model the pressure regulator, we need to model the mass flow rate through orifices, equation of motion for the moving parts, pressure and temperature of the control volumes. To model these governing equations, some assumptions are made which are listed below:

1) The moving parts of the pressure regulators are always in contact, and they move as a single unit. Therefore, moving parts can be modelled as single degree of freedom system which greatly simplifies the dynamic equations.
2) Pressure and temperature of a control volume is uniform.
3) The expansion and compression processes are assumed to be adiabatic.
4) The gas behaves ideally.
5) Seal induced friction force on piston-poppet assembly is assumed to be combination of coulomb and viscous friction.

Pressure regulator is divided into three control volumes. These control volumes (CV) are labelled as CV_{inlet}, CV_{outlet}, and CV_{piston}. This way, state of these control volumes can be calculated separately with pressure and temperature differential equations. Also, there are two ports where mass transfer between the control volumes can occur. Those are named valve orifice and piston orifice. Valve orifice is the main orifice of the pressure regulator where gas flows from inlet to outlet control volume.

Piston orifice is the port that connects outlet and piston control volumes. This orifice allows piston to sense outlet pressure.

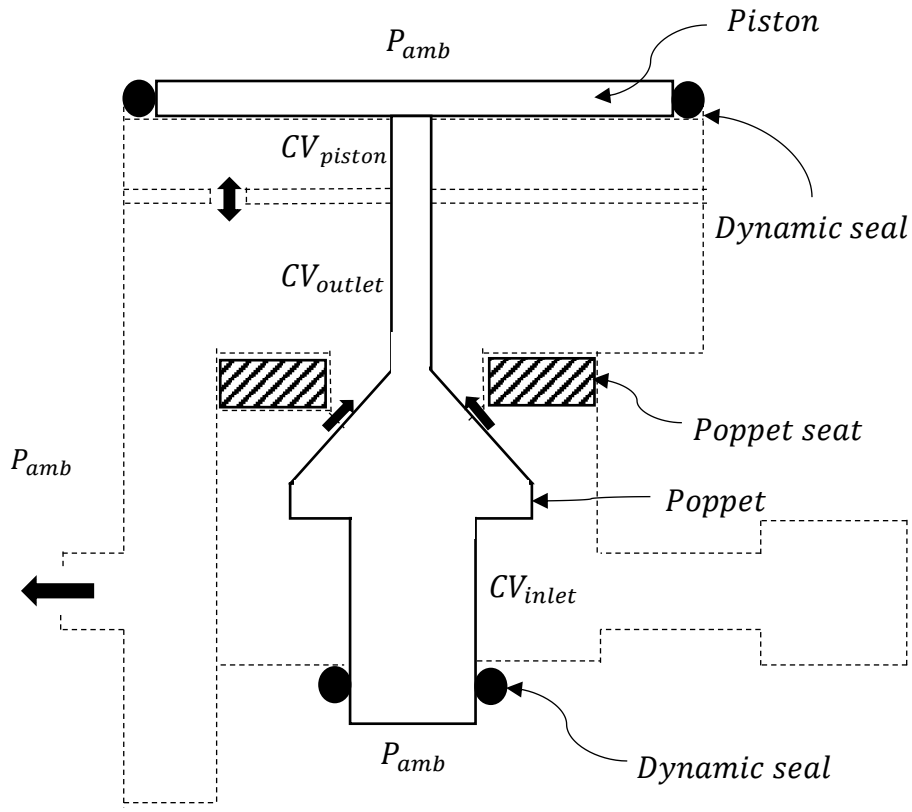

Figure 2.1. Schematic of Control Volumes and Orifices of Mechanical Pressure Regulator

2.1 Governing Equations

2.1.1 Pressure and Temperature Differential Equations

The dynamic differential equations for pressure and temperature of the control volumes were derived from the mass, momentum and energy balance equations, based on the stated assumptions. The analysis is done on a variable control volume

with single inlet and single outlet flow. Variable control volume is due to piston movement, hence it can be modelled as displacement of constant piston area [16]:

$$\frac{dP}{dt} = \frac{\gamma R}{V}(T_{in}\dot{m}_{in} - T\dot{m}_{out}) - \frac{\gamma AP}{V}\dot{x} \tag{2.1}$$

$$\frac{dT}{dt} = \frac{RT^2}{VP}\left[\left(\gamma\frac{T_{in}}{T} - 1\right)\dot{m}_{in} - (\gamma - 1)\dot{m}_{out}\right] - \frac{(\gamma - 1)AT}{V}\dot{x} \tag{2.2}$$

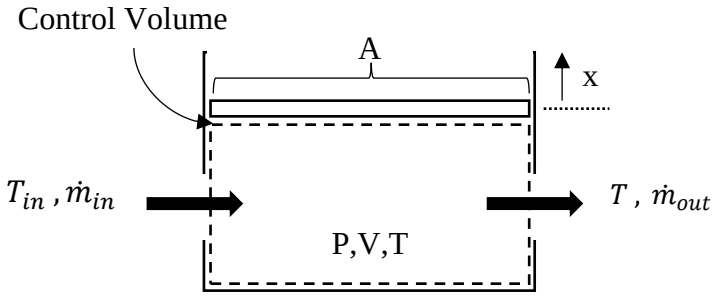

Figure 2.2. Schematic of Control Volume

In equation (2.1) and (2.2), P, V and T are pressure, volume and temperature of the control volume. A is the moving boundary area of the control volume, and amount of movement is denoted by x. $\dot{m}_{in}$ and T_{in} are mass flow rate into the control volume and temperature of the flow, respectively. Similarly, $\dot{m}_{out}$ is mass flow rate out of the control volume. Specific gas constant, R, and ratio of specific heats, γ, are medium specific parameters.

For multiple inlet and outlet flows, corresponding mass flow rate and related temperature terms can be combined:

$$\frac{dP}{dt} = \frac{\gamma R}{V}\left(\sum T_{in}\dot{m}_{in} - \sum T\dot{m}_{out}\right) - \frac{\gamma AP}{V}\dot{x} \tag{2.3}$$

$$\frac{dT}{dt} = \frac{RT^2}{VP}\left[\sum\left(\gamma\frac{T_{in}}{T} - 1\right)\dot{m}_{in} - \sum(\gamma - 1)\dot{m}_{out}\right] - \frac{(\gamma - 1)AT}{V}\dot{x} \tag{2.4}$$

2.1.2 Mass Flow Rate Equation

Flow rate between control volumes through ports can be modelled for a general case of both choked and unchoked flow through orifice [17]:

$$\dot{m} = C_d A f(\gamma) N_{in,out} \frac{P_{in}}{\sqrt{RT_{in}}} \tag{2.5}$$

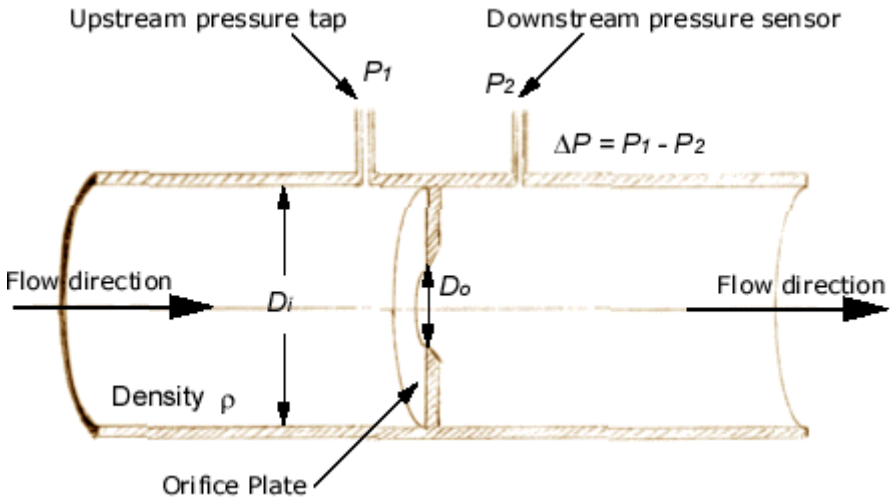

Figure 2.3. Schematic of Mass Flow Rate Through Orifice

In equation (2.5) A is the area of the flow port, subscripts in and out are identifiers according to direction of the mass flow rate.

$f(\gamma)$ is the function of specific heat of the gas only and, can be calculated as follows:

$$f(\gamma) = \sqrt{\gamma} \left(\frac{2}{\gamma + 1}\right)^{(\gamma+1)/[2(\gamma-1)]} \tag{2.6}$$

$N_{in,out}$ is a coefficient that depends on inlet and outlet pressure ratios and specific heat ratio of the gas. For choked flow $N_{in,out} = 1$, else it is less than 1 and it can be calculated as follows:

$$N_{in,out} = N(P_{out}/P_{in}) = \sqrt{\frac{(P_{out}/P_{in})^{2/\gamma} - (P_{out}/P_{in})^{(\gamma+1)/\gamma}}{\frac{\gamma-1}{2}\left(\frac{2}{\gamma+1}\right)^{(\gamma+1)/(\gamma-1)}}} \quad (2.7)$$

Choked flow condition is checked by comparing actual pressure ratio to critical pressure ratio. If the pressure ratio (P_{out}/P_{in}) is less than the P_{crit_ratio} than the flow through orifice can be treated as choked flow. Critical pressure ratio is a function of specific heat ratio of the gas:

$$P_{crit\_ratio} = \left(\frac{2}{\gamma+1}\right)^{\gamma/(\gamma-1)} \quad (2.8)$$

C_d is the discharge coefficient, it can be considered as an empirical correction coefficient for the flow loss of the convective gas due to unsmooth geometry of the orifice. There are numerous studies on approximating the discharge coefficient. Perry [18] established a relationship between upstream and downstream pressure ratio and discharge coefficient. Fleischer [19] and Reid [20] suggested that the discharge coefficient is related with the orifice geometry. Also, Mozer [21] introduced an empirical formula for the discharge coefficient that depends on pressure ratios of upstream and downstream. Even though, assuming C_d to be 1 is a valid approach as Shahani and Aryaei [22] used in their work, in this thesis an approximation by the linear correlation is used based on [17].

$$C_d \approx 1.0 - 0.7(P_{out}/P_{in}) \quad (2.9)$$

2.1.3 Newton's Second Law of Motion

Newton`s second law of motion states: The change of motion is proportional to the motive force impressed; and is made in the direction of the right line in which that force is impressed [23]. From this statement `motion` is assumed as momentum $p$, which is mass times velocity and `change of motion` is interpreted as rate of change of momentum with time [24].

$$\vec{F} = \frac{d}{dt}\vec{p} = \frac{d}{dt}(m\vec{v}) \tag{2.10}$$

For one dimensional analysis, the most famous version of it can be directly written as;

$$F = ma = m\ddot{x} \tag{2.11}$$

Where a is acceleration and x is position of the mass, m.

2.1.4 Magnetic Force in Voice Coil Actuators

Voice coil actuator (VCA) is a type of direct drive linear motor. VCA consists of a permanent-magnetic field assembly and a coil assembly. The current that flows through the coil assembly creates a force vector perpendicular to the direction of the current via interaction with the permanent magnetic field. Commonly used in audio speakers [26] and linear positioning systems [27], voice-coil actuators consist of a permanent magnet and a coil winding connected via a compliant suspension. These two components experience equal and opposite forces proportional to the current applied to the coil [28] [29]; one component is typically attached to the handle, while the other is allowed to move [30].

VCA capability and behaviour should be considered together with its drive circuitry. There are mainly two different topologies for the actuator drive circuit, namely voltage drive, and current drive.

The force generated by the VCA can be modeled with Lorentz force law;

$$F_a = (Bl)i_a \tag{2.12}$$

where B is the magnetic flux density created by the permanent magnet of the actuator, and l is the length of the wire coil that is exposed to the magnetic flux and i_a is the current. Multiplication of B and l is called as force constant of the, FC_{vc}, actuator and has the units N/A.

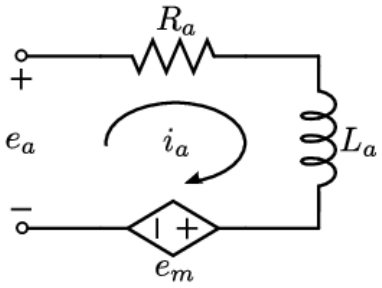

Figure 2.4. VCA electrical schematic

When VCA controlled by the voltage-drive circuit, voltage, e_a, is the directly controlled variable, and the actuator current is controlled indirectly by the actuator`s electromechanical dynamics. For this type of control, actuator current is derived from the following electrical dynamics.

$$e_a = R_a i_a + L_a \frac{di_a}{dt} + e_m \tag{2.13}$$

Where R_a is the resistance of wire, L_a is the inductance of coil, and e_m is the electromotive force (i.e back emf).

When VCA controlled by the current-drive circuit, current, i_a, is the directly controlled variable, and the actuator voltage is controlled indirectly by the actuator`s electromechanical dynamics. For this type of control, the transfer function from the commanded current to actuator force, F_a, simply becomes the force constant of the actuator, FC_{vc}, so this is particularly useful when the actuator force needs to be controlled without concerning about other electrical dynamics.

2.2 Nonlinear Dynamic Model of Hybrid Pressure Regulator

Nonlinear dynamic model of hybrid pressure regulator consists of three control volumes, three mass transfer ports, voice coil actuator with lever mechanism and single degree of freedom moving system. Inlet pressure is assumed to be high reservoir whose pressure and temperature can be controlled as desired. Hence, states of the inlet control volume are not needed to be calculated by pressure and

temperature differential equations. To model the nonlinear system following eight equations should be solved together:

- Pressure and temperature differential equations for each control volume (4 equations)
- Mass flow rate equation for each mass transfer port (3 equations)
- Equation of motion for the single DOF moving system (1 equation)

Resulting dynamic model can be visualized by:

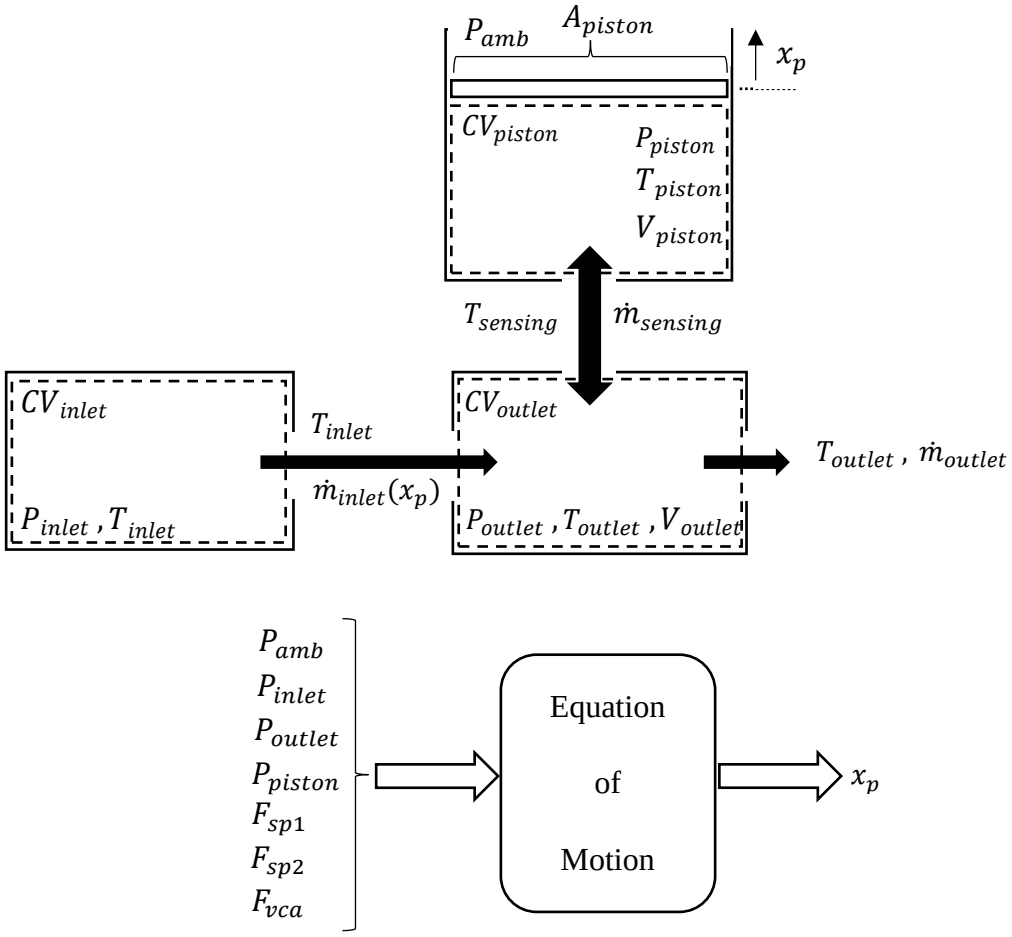

Figure 2.5. Mathematical Model Architecture of Pressure Regulator

Generalized governing equations are adapted to corresponding control volumes and mass flow rate ports and, equation of motion is constructed.

2.2.1 Pressure and Temperature of the Outlet Control Volume

Volume of the outlet chamber is assumed to be constant. Although, the volume of the chamber changes as the position of the moving system changes, the amount of change in volume is negligible compared to initial volume of the outlet chamber.

Outlet chamber has three ports where mass flow into or out of the control volume can occur. These ports are inlet port, outlet port and sensing port. Inlet port is the feeding port of the CV_{outlet}. In normal operation condition inlet pressure is always higher than the outlet pressure, hence direction of the mass flow rate is always from CV_{inlet} to CV_{outlet}. Similarly, ambient pressure is always less than the outlet pressure, hence direction of the mass flow rate is always from $CV_{outlet}$to ambient (i.e. atmosphere). Sensing port is located in between CV_{piston} and CV_{outlet}. The direction of mass flow rate through sensing port depends on the pressure gradient between these control volumes.

With these considerations in mind, we can write pressure and temperature differential equations for the CV_{outlet} as follows:

If $P_{outlet} > P_{piston}$, mass flow through the sensing port, $\dot{m}_{sensing}$, is out of CV_{outlet}:

$$\frac{dP_{outlet}}{dt} = \frac{\gamma R}{V_{outlet}}\left(T_{inlet}\dot{m}_{inlet} - T_{outlet}(\dot{m}_{outlet} + \dot{m}_{sensing})\right) \tag{2.14}$$

$$\frac{dT_{outlet}}{dt} = \frac{RT_{outlet}^2}{V_{outlet}P_{outlet}}\left[\left(\gamma\frac{T_{inlet}}{T_{outlet}} - 1\right)\dot{m}_{inlet} - (\gamma - 1)(\dot{m}_{outlet} + \dot{m}_{sensing})\right] \tag{2.15}$$

If $P_{outlet} < P_{piston}$, mass flow through the sensing port is towards CV_{outlet}:

$$\frac{dP_{outlet}}{dt} = \frac{\gamma R}{V_{outlet}}\left(T_{inlet}\dot{m}_{inlet} - T_{outlet}\dot{m}_{outlet} + T_{piston}\dot{m}_{sensing}\right) \tag{2.16}$$

$$\frac{dT_{outlet}}{dt} = \frac{RT_{outlet}^2}{V_{outlet}P_{outlet}}\left[\left(\gamma\frac{T_{inlet}}{T_{outlet}} - 1\right)\dot{m}_{inlet} - (\gamma - 1)\dot{m}_{outlet} + \left(\gamma\frac{T_{sensing}}{T_{outlet}} - 1\right)\dot{m}_{sensing}\right] \tag{2.17}$$

2.2.2 Pressure and Temperature of the Piston Control Volume

Volume of the piston chamber changes as the piston moves. Noting that, the sign convention for the moving piston-poppet assembly is opposite of the generalized approach for the variable control volume analysis. Hence, the velocity term in pressure and temperature equations changes sign. Also, the volume of the piston chamber is a function of the piston position which should be taken into consideration.

Control volume has single port where mass flow occurs between CV_{outlet} and CV_{piston} according to the pressure gradient between these two control volumes.

With these considerations in mind, we can write pressure and temperature differential equations for the CV_{piston} as follows:

If $P_{outlet} > P_{piston}$, mass flow through the sensing port is into the piston CV:

$$\frac{dP_{piston}}{dt} = \frac{\gamma R}{V_{piston}}T_{outlet}\dot{m}_{sensing} + \frac{\gamma A_{piston,l}P_{piston}}{V_{piston}}\dot{x}_p \tag{2.18}$$

$$\frac{dT_{piston}}{dt} = \frac{RT_{piston}^2}{V_{piston}P_{piston}}\left[\left(\gamma\frac{T_{outlet}}{T_{piston}} - 1\right)\dot{m}_{sensing}\right] + \frac{(\gamma - 1)A_{piston,l}T_{piston}}{V_{piston}}\dot{x}_p \tag{2.19}$$

If $P_{outlet} < P_{piston}$, mass flow through the sensing port is out of the piston CV:

$$\frac{dP_{piston}}{dt} = \frac{\gamma R}{V_{piston}}(-T_{piston}\dot{m}_{sensing}) + \frac{\gamma A_{piston,l} P_{piston}}{V_{piston}}\dot{x}_p \tag{2.20}$$

$$\frac{dT_{piston}}{dt} = \frac{RT_{piston}^2}{V_{piston}P_{piston}}\left[-(\gamma-1)\dot{m}_{sensing}\right] + \frac{(\gamma-1)A_{piston,l}T_{piston}}{V_{piston}}\dot{x}_p \tag{2.21}$$

In equation (2.18) to (2.21), V_{piston} can be calculated as:

$$V_{piston} = V_{piston,0} - A_{piston,l}(x - x_{design}) \tag{2.22}$$

2.2.3 Mass Flow Rate Through the Inlet Port

Inlet port is the feeder port of the outlet control volume. It is a port where the regulation of the outlet pressure happens. According to position of the poppet-piston assembly, effective flow area of the inlet port changes, thus mass flow rate through the inlet port varies. Hence, mass flow rate through the inlet port depends on the position of poppet-piston assembly, namely x_p.

$$\dot{m}_{inlet} = C_{d,i}A_i(x_p)f(\gamma)N_{inlet,outlet}\frac{P_{inlet}}{\sqrt{RT_{inlet}}} \tag{2.23}$$

In order to model the mass flow rate, effective flow area should be calculated.

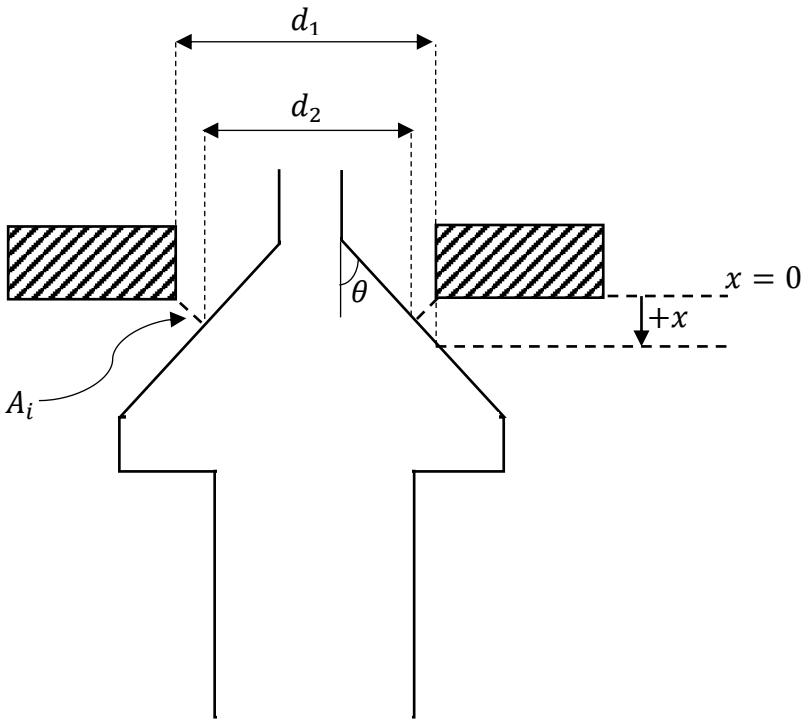

Figure 2.6. Orifice Area Between the Poppet and Seat

A_i has a truncated conical shape whose large diameter is d_1, small diameter is d_2 and height, h, is the perpendicular opening of the port and θ is seat angle. Therefore, area of the inlet port can be calculated as:

$$A_i(x) = 0.5\pi(d_1 + d_2)\sqrt{h^2 + 0.25(d_1 - d_2)^2} \tag{2.24}$$

In equation (2.24) d_2 and h can be calculated as:

$$d_2 = d_1 - 2x_p sin\theta cos\theta \tag{2.25}$$

$$h = x_p sin^2(\theta) \tag{2.26}$$

Then equation (2.24) can be rewritten as:

$$A_i(x) = \pi x sin\theta(d_1 - x_p sin\theta cos\theta) \tag{2.27}$$

Also, $C_{d,i}$ can be estimated from:

$$C_{d,i} \approx 1.0 - 0.7(P_{outlet}/P_{inlet}) \tag{2.28}$$

Another term in the mass flow rate equation is $f(\gamma)$ which is a function of specific heats ratio of the gas, and it can be calculated by (2.6).

The flow from inlet to outlet is assumed to be choked flow for all operational conditions. Hence, $N_{in,out}$ is taken as 1.

2.2.4 Mass Flow Rate Through the Sensing Port

Sensing port allows the mass transfer between outlet and piston chambers so that piston chamber can sense outlet pressure. Port has a fixed circular area. Direction of the mass flow rate depends on the sign of pressure difference between CV_{outlet} and CV_{piston}. Since pressure of those control volumes are expected to be close to each other, flow direction can change quite frequently.

If $P_{outlet} > P_{piston}$, mass flow through the sensing port is into the CV_{piston}:

$$\dot{m}_{sensing} = C_{d,s} A_s f(\gamma) N_{outlet,piston} \frac{P_{outlet}}{\sqrt{RT_{outlet}}} \tag{2.29}$$

Corresponding discharge coefficient can be calculated from:

$$C_{d,s} \approx 1.0 - 0.7(P_{piston}/P_{outlet}) \tag{2.30}$$

If $P_{outlet} < P_{piston}$,, mass flow through the sensing port is out of the CV_{piston}:

$$\dot{m}_{sensing} = C_{d,s} A_s f(\gamma) N_{piston,outlet} \frac{P_{piston}}{\sqrt{RT_{piston}}} \tag{2.31}$$

Corresponding discharge coefficient can be calculated from:

$$C_{d,s} \approx 1.0 - 0.7(P_{outlet}/P_{piston}) \tag{2.32}$$

In equation (2.29) and (2.30), V_{piston} can be calculated as:

$$A_s = \pi \frac{d_s^2}{4} \tag{2.33}$$

Since P_{piston} and P_{outlet} are always close to each other, their ratio is close to 1 which means the pressure ratio of downstream and upstream in higher than the critical pressure ratio calculated by equation (2.8). Therefore, $N_{outlet,piston}$ and $N_{piston,outlet}$ terms are not equal to 1 and should be calculated by using equation (2.7).

2.2.5 Mass Flow Rate Through the Outlet Port

Mass flow rate demand of the application is met by the flow through the outlet port. In most cases, application may require different mass flow rates hence it has adjustable total flow area. Therefore, the mass flow rate area of the outlet port may not be constant but can be controlled by a higher control authority.

$$\dot{m}_{outlet} = C_{d,o} A_o f(\gamma) N_{outlet,amb} \frac{P_{outlet}}{\sqrt{RT_{outlet}}} \tag{2.34}$$

Here, P_{amb} is either atmospheric pressure or close to vacuum pressure for space applications. P_{amb} to P_{outlet} is generally less than the critical pressure ratio (see equation (2.8)), which makes the flow choked and, $N_{outlet,amb}$ can be taken as 1.

However, for most applications mass flow rate is the explicit design parameter and corresponding outlet port area is calculated and with respect to required mass flow rate. Consequently, requirement of a pressure regulator mostly stated according to mass flow rate, instead of outlet orifice area. Therefore, in this thesis while simulating the pressure regulator, mass flow rate through outlet port is not calculated according to outlet port area, instead mass flow rate through the outlet port is directly enforced.

2.2.6 Electronic Actuation Model

Pneumatic forces are higher than the electromagnetic forces especially at high pressures, on the other hand required stroke of the designed pressure regulator does

not go beyond one milimeter. Thus, a lever mechanism is utilized to gain advantage of the full stroke of voice coil actuator and to increase its effective control force on the moving assembly.

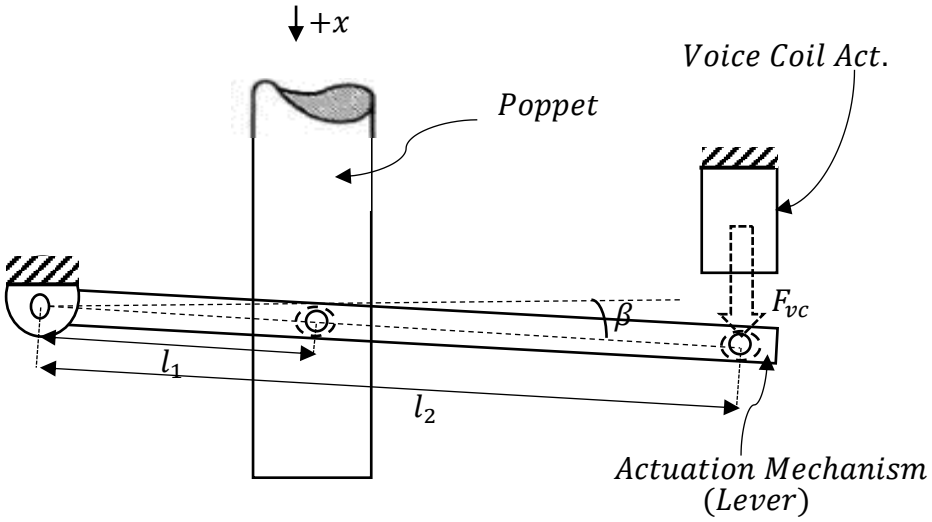

Figure 2.7. Voice Coil Actuator Lever Mechanism

Current of the voice coil actuator is used as the controlled input. Hence, as discussed on 2.1.4, voice coil force can be modelled using Lorentz force law:

$$F_{vca} = (Bl)i_{vc} \tag{2.35}$$

Where (Bl) multiplication is known as `force constant`, Fc_{vca}, of the voice coil actuator and it is generally indicated directly as a specification for a commercially available voice coil actuator.

2.2.7 Equation of Motion for the Moving System

Motion of the moving parts are modelled together as single degree of freedom system with includes piston, poppet, springs, actuation mechanism and voice coil core.

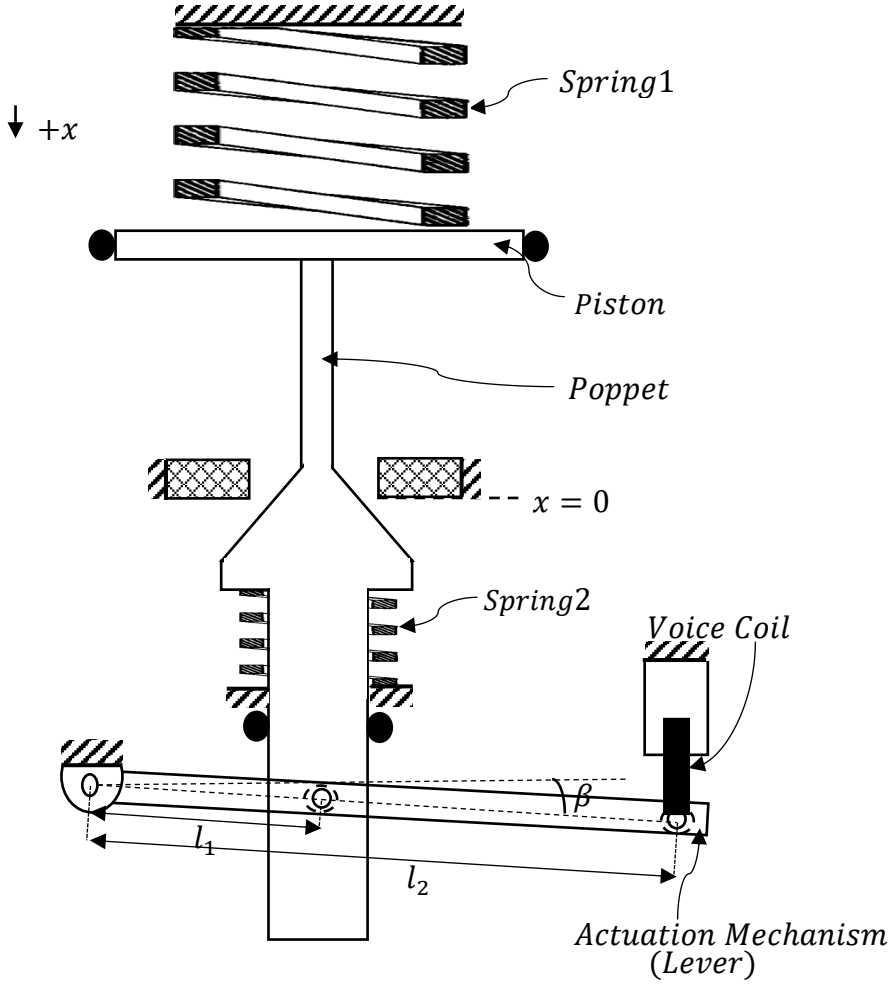

Figure 2.8. Moving Components of Hybrid Pressure Regulator

From Figure 2.8 it is shown that main movement of the hybrid pressure regulator is along the x axis where the movement of springs, poppet and piston takes place. Movement of voice coil is related to movement of poppet by the lever angle, β, and their respective lever arms, l_2 and l_1. Mass center of the lever is located $l_2/2$ away from the pivot point.

At this point a simplification is made by lumping the total rotational inertia of lever and and voice coil actuator on to x-axis as a translational mass by using lever ratio. This simplification is justified since the lever angle, β, is always small(within $\mp 5°$) around the operating stroke range of the poppet.

Therefore, actuation mass can be defined as;

$$m_{actuation} = \frac{m_{lever}(l_2/2)^2 + m_{vc}l_2^2}{l_1^2} \tag{2.36}$$

Effective mass of the springs along the x-axis can be taken as $1/3$ of the actual mass of the springs [25].

$$m_{springs} = \frac{m_{sp1} + m_{sp2}}{3} \tag{2.37}$$

Finally, equivelant mass of the whole moving system along the x-axis can be used as:

$$m_{eq} = m_{piston} + m_{poppet} + m_{springs} + m_{actution} \tag{2.38}$$

Equation of motion of the moving parts is formed by inspecting the net force on the system. Free body diagram:

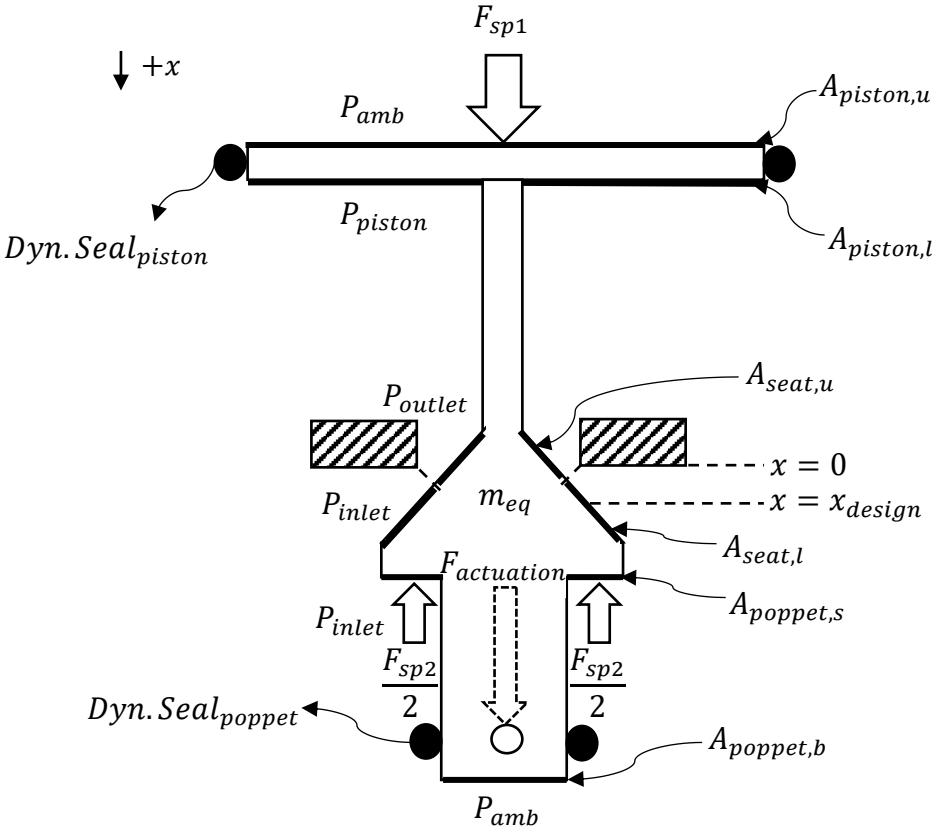

Figure 2.9. Free Body Diagram of the Moving Parts

Note the equation of motion on the x-axis is of interest. Hence, by $A_{seat,u}$ and $A_{seat,l}$ only the projection area that is perpendicular to x-axis is considered.

Net force can be written as:

$$\begin{aligned} F_{net} = {} & F_{sp1} + P_{amb}A_{piston,u} - P_{piston}A_{piston,l} + P_{outlet}A_{seat,u} \\ & + P_{inlet}A_{seat,l} - P_{inlet}A_{poppet,s} - F_{sp2} \\ & - P_{amb}A_{poppet,b} - F_{fric} + F_{actuation} \end{aligned} \tag{2.39}$$

Spring forces can be described as:

$$F_{sp1} = F_{sp1,pre} + k_1(x_{design} - x), \quad F_{sp1,pre} = k_1\delta_{sp1,pre} \tag{2.40}$$

$$F_{sp2} = F_{sp2,pre} + k_2(x - x_{design}), \quad F_{sp2,pre} = k_2\delta_{sp2,pre} \tag{2.41}$$

Terms $\delta_{sp1,pre}$ and $\delta_{sp2,pre}$ are the amount of initial compressions of the spring1 and spring2 respectively, when the position of the moving assembly is equal to x_{design}.

And friction force can be estimated as the combination of coulumb and viscous effects created by dynamic seals that are located at piston circumference and poppet circumference. Total friction force is modelled as;

$$F_{fric} = sgn(\dot{x})(F_{coul,poppet} + F_{coul,piston}) + c\dot{x} \tag{2.42}$$

Poppet and piston friction forces can be combined.

$$F_{coulomb} = F_{coul,poppet} + F_{coul,piston} \tag{2.43}$$

$F_{coul,poppet}$ is a function of P_{inlet} and $F_{coul,piston}$ is a function of P_{piston}. See Appendix A for the estimation of friction force.

In equation (2.39) mentioned effective control actuation force is defined below.

$$F_{actuation} = r_{lever}F_{vca} \tag{2.44}$$

Voice coil force is amplified by an actuatıın mechanism whose lever ratio is defined as:

$$r_{lever} = \frac{l_2}{l_1} \tag{2.45}$$

Rearranging equations (2.39), (2.40) and (2.41) equation of motion can be written as:

$$\begin{aligned} F_{sp1,pre} + P_{amb}A_{piston,u} - P_{piston}A_{piston,l} + P_{outlet}A_{seat,u} \\ + P_{inlet}A_{seat,l} - P_{inlet}A_{poppet,s} - F_{sp2,pre} \\ - P_{amb}A_{poppet,b} - sgn(\dot{x})F_{coulomb} + F_{actuation} \\ = m_{eq}\ddot{x} + c\dot{x} + k_{eq}x \end{aligned} \tag{2.46}$$

Springs are in parallel connection hence the equivalent spring stiffness is:

$$k_{eq} = k_1 + k_2 \tag{2.47}$$

2.2.8 Simplified Nonlinear Dynamic Model

Simplifications are made to achieve the linearized model of the system. By combining the CV_{piston} with the CV_{outlet}, modelling effort for the flow rate through the sensing port is avoided. The reason of this simplification is the nonlinearity caused by the flow direction which can change during operation according to pressures of the specified control volumes. This simplification is justified since pressure and temperature values of those control volumes are always close to each other, especially when the sensing port area is large enough. Also, the volume of the outlet chamber is big enough to ignore any volume changes due to piston movement, therefore combined control volume assumed to has a constant volume. Simplified pressure regulator model has the following structure in terms of control volume and mass flow ports between those control volumes.

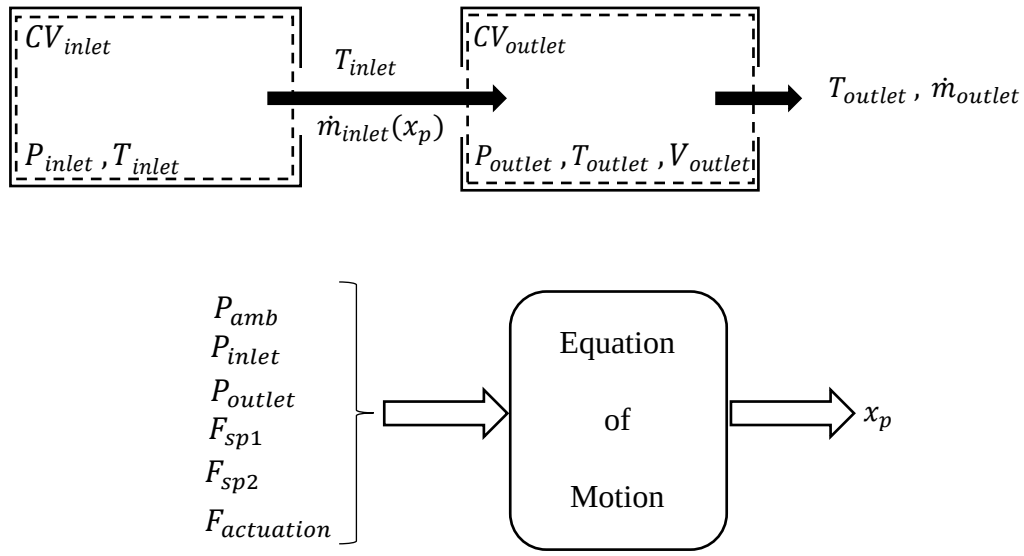

Figure 2.10. Architecture for the Simplified Nonlinear Pressure Regulator Model

With mentioned simplifications new nonlinear governing equations are:

$$\dot{P}_{outlet} = \frac{\gamma R}{V_{outlet}}(T_{inlet}\dot{m}_{inlet} - T_{outlet}\dot{m}_{outlet}) = f_1(\underline{x}, \underline{d}, u) \tag{2.48}$$

$$\dot{T}_{outlet} = \frac{RT_{outlet}^2}{V_{outlet}P_{outlet}}\left[\left(\gamma\frac{T_{inlet}}{T_{outlet}} - 1\right)\dot{m}_{inlet} - (\gamma - 1)\dot{m}_{outlet}\right] = f_2(\underline{x}, \underline{d}, u) \tag{2.49}$$

$$\dot{x}_p = x_4 = f_3(\underline{x}, \underline{d}, u) \tag{2.50}$$

$$\ddot{x}_p = \left\{ \begin{array}{c} P_{amb}(A_{piston,u} - A_{poppet,b}) \\ +P_{outlet}\left(A_{seat,u} - A_{piston,l}\right) \\ +P_{inlet}(A_{seat,l} - A_{poppet,s}) \\ +F_{sp1,pre} - F_{sp2,pre} - c\dot{x}_p - (k_1 + k_2)x_p \\ +r_{lever} F c_{vca} i_{vc} \end{array} \right\} / m_{eq} = f_4\left(\underline{x}, \underline{d}, u\right) \quad (2.51)$$

State vector, $\underline{x}$, disturbance vector, $\underline{d}$, and control input, u, for nonlinear system of equations from equation (2.48) to (2.51) are shown:

$$\underline{x} = \begin{bmatrix} P_{outlet} \\ T_{outlet} \\ x_p \\ \dot{x}_p \end{bmatrix}, \ \underline{d} = \begin{bmatrix} P_{inlet} \\ T_{inlet} \\ \dot{m}_{outlet} \end{bmatrix}, u = i_{vc} \quad (2.52)$$

2.3 Linearization of Dynamic Model

Simplified nonlinear dynamic model of the mechanical pressure regulator is linearized around the steady state nominal operation point. Nominal operation point is selected such that it represents the dynamic model of the pressure regulator to the best degree within the whole operational envelope. There are three main variables that describe the operational envelope. These are non-constant inlet pressure and temperature, and various mass flow rate demands out of the pressure regulator.

Variables at the steady state nominal operation point is denoted with asterisk (*) sign.

State variables of the linearized system are defined as:

$$\underline{x}^* = \begin{bmatrix} \Delta P_{outlet} \\ \Delta T_{outlet} \\ \Delta x_p \\ \Delta \dot{x}_p \end{bmatrix} = \begin{bmatrix} P_{outlet} - {P_{outlet}}^* \\ T_{outlet} - {T_{outlet}}^* \\ x_p - x_p^* \\ \dot{x}_p - {\dot{x}_p}^* \end{bmatrix} \quad (2.53)$$

Disturbances to the linearized system is defined as:

$$\underline{d}^* = \begin{bmatrix} \Delta P_{inlet} \\ \Delta T_{inlet} \\ \Delta \dot{m}_{outlet} \end{bmatrix} = \begin{bmatrix} P_{inlet} - {P_{inlet}}^* \\ T_{inlet} - {T_{inlet}}^* \\ \dot{m}_{outlet} - {\dot{m}_{outlet}}^* \end{bmatrix} \tag{2.54}$$

And the only control input is defined as:

$$u^* = i_{vc} - {i_{vc}}^* \tag{2.55}$$

Now plant model can be created in state space form:

$$\begin{gathered} \dot{\underline{x}}^* = \overline{A}\underline{x}^* + \underline{b}\, u^* + \overline{F}\underline{d}^* \\ \mathrm{y} = \underline{c}\, \underline{x}^* \end{gathered} \tag{2.56}$$

In order to form the system matrices of the linearized plant model, Jacobian of the system should be written:

$$J(\underline{x}, \underline{d}, u) = \begin{bmatrix} \frac{\partial f_1(\underline{x},\underline{d},u)}{\partial x_1} & \cdots & \frac{\partial f_1(\underline{x},\underline{d},u)}{\partial x_4} & \frac{\partial f_1(\underline{x},\underline{d},u)}{\partial d_1} & \cdots & \frac{\partial f_1(\underline{x},\underline{d},u)}{\partial d_3} & \frac{\partial f_1(\underline{x},\underline{d},u)}{\partial u} \\ \frac{\partial f_2(\underline{x},\underline{d},u)}{\partial x_1} & \cdots & \frac{\partial f_2(\underline{x},\underline{d},u)}{\partial x_4} & \frac{\partial f_2(\underline{x},\underline{d},u)}{\partial d_1} & \cdots & \frac{\partial f_2(\underline{x},\underline{d},u)}{\partial d_3} & \frac{\partial f_2(\underline{x},\underline{d},u)}{\partial u} \\ \frac{\partial f_3(\underline{x},\underline{d},u)}{\partial x_1} & \cdots & \frac{\partial f_3(\underline{x},\underline{d},u)}{\partial x_4} & \frac{\partial f_3(\underline{x},\underline{d},u)}{\partial d_1} & \cdots & \frac{\partial f_3(\underline{x},\underline{d},u)}{\partial d_3} & \frac{\partial f_3(\underline{x},\underline{d},u)}{\partial u} \\ \frac{\partial f_4(\underline{x},\underline{d},u)}{\partial x_1} & \cdots & \frac{\partial f_4(\underline{x},\underline{d},u)}{\partial x_4} & \frac{\partial f_4(\underline{x},\underline{d},u)}{\partial d_1} & \cdots & \frac{\partial f_4(\underline{x},\underline{d},u)}{\partial d_3} & \frac{\partial f_4(\underline{x},\underline{d},u)}{\partial u} \end{bmatrix} \tag{2.57}$$

Evaluating Jacobian around the nominal operation point yields the system matrixes:

$$\bar{A} = \left[\begin{matrix} \frac{\partial f_1(\underline{x},\underline{d},u)}{\partial x_1} & \frac{\partial f_1(\underline{x},\underline{d},u)}{\partial x_2} & \frac{\partial f_1(\underline{x},\underline{d},u)}{\partial x_3} & \frac{\partial f_1(\underline{x},\underline{d},u)}{\partial x_4} \\ \frac{\partial f_2(\underline{x},\underline{d},u)}{\partial x_1} & \frac{\partial f_2(\underline{x},\underline{d},u)}{\partial x_2} & \frac{\partial f_2(\underline{x},\underline{d},u)}{\partial x_3} & \frac{\partial f_2(\underline{x},\underline{d},u)}{\partial x_4} \\ \frac{\partial f_3(\underline{x},\underline{d},u)}{\partial x_1} & \frac{\partial f_3(\underline{x},\underline{d},u)}{\partial x_2} & \frac{\partial f_3(\underline{x},\underline{d},u)}{\partial x_3} & \frac{\partial f_3(\underline{x},\underline{d},u)}{\partial x_4} \\ \frac{\partial f_4(\underline{x},\underline{d},u)}{\partial x_1} & \frac{\partial f_4(\underline{x},\underline{d},u)}{\partial x_2} & \frac{\partial f_4(\underline{x},\underline{d},u)}{\partial x_3} & \frac{\partial f_4(\underline{x},\underline{d},u)}{\partial x_4} \end{matrix} \right]_{\substack{x_1={P_{outlet}}^* \\ x_2={T_{outlet}}^* \\ x_3=x_p^* \\ x_4={\dot{x}_p}^* \\ d_1={P_{inlet}}^* \\ d_2={T_{inlet}}^* \\ d_3={\dot{m}_{outlet}}^* \\ u={i_{vc}}^*}} \tag{2.58}$$

$$\bar{F} = \left[\begin{matrix} \frac{\partial f_1(\underline{x},\underline{d},u)}{\partial d_1} & \frac{\partial f_1(\underline{x},\underline{d},u)}{\partial d_2} & \frac{\partial f_1(\underline{x},\underline{d},u)}{\partial d_3} \\ \frac{\partial f_2(\underline{x},\underline{d},u)}{\partial d_1} & \frac{\partial f_2(\underline{x},\underline{d},u)}{\partial d_2} & \frac{\partial f_2(\underline{x},\underline{d},u)}{\partial d_3} \\ \frac{\partial f_3(\underline{x},\underline{d},u)}{\partial d_1} & \frac{\partial f_3(\underline{x},\underline{d},u)}{\partial d_2} & \frac{\partial f_3(\underline{x},\underline{d},u)}{\partial d_3} \\ \frac{\partial f_4(\underline{x},\underline{d},u)}{\partial d_1} & \frac{\partial f_4(\underline{x},\underline{d},u)}{\partial d_2} & \frac{\partial f_4(\underline{x},\underline{d},u)}{\partial d_3} \end{matrix}\right]\Bigg|_{\substack{x_1=P_{outlet}^* \\ x_2=T_{outlet}^* \\ x_3=x_p^* \\ x_4=\dot{x}_p^* \\ d_1=P_{inlet}^* \\ d_2=T_{inlet}^* \\ d_3=\dot{m}_{outlet}^* \\ u=i_{vc}^*}} \tag{2.59}$$

$$\underline{b} = \left[\begin{matrix} \frac{\partial f_1(\underline{x},\underline{d},u)}{\partial u} \\ \frac{\partial f_2(\underline{x},\underline{d},u)}{\partial u} \\ \frac{\partial f_3(\underline{x},\underline{d},u)}{\partial u} \\ \frac{\partial f_4(\underline{x},\underline{d},u)}{\partial u} \end{matrix}\right]\Bigg|_{\substack{x_1=P_{outlet}^* \\ x_2=T_{outlet}^* \\ x_3=x_p^* \\ x_4=\dot{x}_p^* \\ d_1=P_{inlet}^* \\ d_2=T_{inlet}^* \\ d_3=\dot{m}_{outlet}^* \\ u=i_{vc}^*}} \tag{2.60}$$

Only measured feedback is assumed to be P_{outlet} hence, $\underline{c}$ becomes the following:

$$\underline{c} = [1 \quad 0 \quad 0 \quad 0] \tag{2.61}$$

CHAPTER 3

CONTROLLER DESIGN

A controller is needed to achieve the desired outlet pressure regulation performance with actuation of voice coil. To design and tune the controller hypotetical but realistic operational condition for a pressure regulator is described. Linearization point for the described operational envelope is selected and linerized state space model around the linerization point is formed. PI controller for the linearized model is designed and tuned by using the non-linear model.

3.1 Operational Envelope

Nominal outlet pressure of the pressure regulator should be set to $30\ bar$ and it should operate under different conditions. Those conditions are:

- During operation inlet pressure can change between $60 - 300\ bar$
- During operation inlet temprature can change between $230 - 330°K$
- During operation mass flow rate at the downstream of the pressure regulator can change between $0.010 - 0.090\ kg/s$
- Medium is Helium

3.2 Parameters

Properties of flow media for the defined operational envelope is evaluated and pressure regulator is designed such that regulation accuracy is optimized while keeping the design physically realisable and logical in terms of mass and geometrical factors.

Parameters that are used during simulation can be grouped by flow media parameters, pressure regulator parameters, spring parameters and actuation mechanism parameters and listed below.

Table 3.1 Simulation Parameters

Description	Symbol	Value	Unit
Medium Parameters (He)			
Individual gas constant	R	2077	$J/(kgK)$
Ratio of specific heats	γ	1.667	-
Parameters of Pressure Regulator			
Diameter of the poppet seat	d_1	11.8	mm
Poppet seat angle	θ	45	°
Area of upper side of the piston	$A_{piston,u}$	1257	mm^2
Area of lower side of the piston	$A_{piston,l}$	1250	mm^2
Area of upper side of the poppet near seat	$A_{seat,u}$	102	mm^2
Area of lower side of the poppet near seat	$A_{seat,l}$	92	mm^2
Area of shoulder of the poppet	$A_{poppet,s}$	92	mm^2
Area of bottom of the poppet	$A_{poppet,b}$	109	mm^2
Stroke at the design point	x_{design}	0.17	mm
Initial volume of sensing chamber at x_{design}	$V_{piston,0}$	0.006	L
Volume of outlet chamber	V_{outlet}	50	L
Sense port area	A_{sense}	3	mm^2
Mass of poppet	m_{poppet}	20	g
Mass of piston	m_{piston}	80	g
Coulumb Friction	$F_{coulomb}$	66	N
Damping coefficient	c	515	Nm/s
Spring Parameters			
Mass of the first spring	m_{sp1}	154	g

Table 3.1 Simulation Parameters (cont'd)

Stiffness of the first spring	k_1	212	N/mm
Precompression at x_{design} of the first spring	$\delta_{sp1,pre}$	17.3	mm
Mass of the second spring	m_{sp2}	7	g
Stiffness of the second spring	k_2	54	N/mm
Precompression at x_{design} of the second spring	$\delta_{sp2,pre}$	6.2	mm
Actuation Mechanism Parameters			
Mass of lever	m_{lever}	10	g
Moving mass of voice coil	m_{vc}	85	g
Lever length up to poppet	l_1	6	mm
Lever length up to voice coil	l_2	48	mm
Voice coil force constant	Fc_{vc}	34	N/A
Voice coil saturation current	i_{vc_sat}	0.8	A
Voice coil max. stroke	x_{vc_sat}	8	mm

3.3 Linearized Model

Dynamic model of the hybrid pressure regulator is inherently non-linear. Linearizing the model around an operating point that can be used the analyse the system or design a controller is a common approach. For the hybrid pressure regulator linearization point is chosen as the point where it can be used to analyse the whole described operational envelope using the methodology explained on section 2.3. Parameters of linearization point that yields a representative system dynamic for the full operational envelope is shown below:

Table 3.2 Linearization Point for Nominal Operating Condition

Parameter	Value	Unit
States		
P_{outlet}^{*}	30	bar
T_{outlet}^{*}	280	$°K$
x^{*}	0.167	mm
$\dot{x}^{*}$	0	mm/s
Disturbances		
P_{inlet}^{*}	140	bar
T_{inlet}^{*}	280	$°K$
$\dot{m}_{outlet}^{*}$	50	g/s
Control		
i_{vc}^{*}	0	A

Plugging in these values into equations (2.58) to (2.61) yields the following matrices:

$$\overline{A} = \begin{bmatrix} -0.035 & -2.164x10^{3} & 3.548x10^{9} & 0 \\ -1.331x10^{-6} & -0.202 & 1.325x10^{5} & 0 \\ 0 & 0 & 0 & 1 \\ -1.025x10^{-4} & 0 & -4.562x10^{4} & -88.45 \end{bmatrix} \tag{3.1}$$

$$\underline{b} = \begin{bmatrix} 0 \\ 0 \\ 0 \\ 46.647 \end{bmatrix} \tag{3.2}$$

$$\overline{F} = \begin{bmatrix} 0.051 & 1.082x10^{3} & -1.212x10^{7} \\ 1.902x10^{-6} & 0.162 & -452.551 \\ 0 & 0 & 0 \\ 0 & 0 & 0 \end{bmatrix} \tag{3.3}$$

$$\underline{c} = [1 \quad 0 \quad 0 \quad 0] \tag{3.4}$$

It is useful to combine control and disturbances in a single vector, this leads to simplified representation in state space form which can be seen below:

$$\underline{\dot{x}}^* = \overline{A}\underline{x}^* + \overline{B}\begin{bmatrix} u^* \\ \underline{d}^* \end{bmatrix} \tag{3.5}$$

$$y = \underline{c}\ \underline{x}^* \tag{3.6}$$

Writing equations (3.5) and (3.6) in open form and plugging in the numerical values yields:

$$\begin{bmatrix} \Delta\dot{P}_{outlet} \\ \Delta\dot{T}_{outlet} \\ \Delta\dot{x} \\ \Delta\ddot{x} \end{bmatrix} = \begin{bmatrix} -0.035 & -2.164x10^{3} & 3.548x10^{9} & 0 \\ -1.331x10^{-6} & -0.202 & 1.325x10^{5} & 0 \\ 0 & 0 & 0 & 1 \\ -1.025x10^{-4} & 0 & -4.562x10^{4} & -88.45 \end{bmatrix} \begin{bmatrix} \Delta P_{outlet} \\ \Delta T_{outlet} \\ \Delta x \\ \Delta\dot{x} \end{bmatrix} + \begin{bmatrix} 0 & 0.051 & 1.082x10^{3} & -1.212x10^{7} \\ 0 & 1.902x10^{-6} & 0.162 & -452.551 \\ 0 & 0 & 0 & 0 \\ 46.647 & 0 & 0 & 0 \end{bmatrix} \begin{bmatrix} i_{vc} \\ \Delta P_{inlet} \\ \Delta T_{inlet} \\ \Delta\dot{m}_{outlet} \end{bmatrix} \tag{3.7}$$

$$\Delta P_{outlet} = [1 \quad 0 \quad 0 \quad 0] \begin{bmatrix} \Delta P_{outlet} \\ \Delta T_{outlet} \\ \Delta x \\ \Delta\dot{x} \end{bmatrix} \tag{3.8}$$

3.4 Controller Design

Two different controllers are designed for different hybrid pressure regulator models. The first controller is designed by using linearized plant model and the second controller is designed directly for the nonlinear model. The biggest difference between those models is the effect of friction. The nonlinear model that includes friction model requires different controller than the controller designed with linearized model since friction affects the system dynamics of the plant.

3.4.1 Controlled Design with Linearized Model

Proportional-Integral (PI) controller is designed to control the voice coil actuator to achieve the high-pressure control accuracy. Controller is designed by using a linearized model, however linearization point is not selected as nominal operating point, instead linearization point is chosen by considering extreme of the operation envelope where inlet pressure and temperature are at their highest and mass flow rate demand is at its lowest. The reason behind this selection is, it leads to minimum gain margin when linearized. Hence, if controller gains are selected according to this extreme condition, we can guarantee the stability for the rest of the operational envelope. Linearization point for the controller design is shown below:

Table 3.3 Linearization Point for Controller Design

Parameter	Value	Unit
States		
${P_{outlet}}^{*cd}$	31	bar
${T_{outlet}}^{*cd}$	330	$°K$
x^{*cd}	0.008	mm
$\dot{x}^{*cd}$	0	mm/s
Disturbances		
${P_{inlet}}^{*cd}$	300	bar
${T_{inlet}}^{*cd}$	330	$°K$
${\dot{m}_{outlet}}^{*cd}$	10	g/s
Control		
${i_{vc}}^{*cd}$	0	A

Plant can be linearized with this new linearization point as following the same methodology done in section 3.3 to achieve system matrices $\overline{A}$, $\overline{B}$ and $\underline{c}$.

Transfer function between the current command and outlet pressure is formed using the state space form.

$$\underline{G}(s) = \underline{c}(s\overline{I} - \overline{A})^{-1}\overline{B} \tag{3.9}$$

Identity matrix is fourth order.

$$\overline{I} = \begin{bmatrix} 1 & 0 & 0 & 0 \\ 0 & 1 & 0 & 0 \\ 0 & 0 & 1 & 0 \\ 0 & 0 & 0 & 1 \end{bmatrix} \tag{3.10}$$

This yields four different transfer functions since we combined input and disturbances into one vector. The transfer function from voice coil current command to outlet pressure is of interest which is shown below.

$$G_{iP}(s) = \frac{4.258x10^{11}s + 1.177x10^{10}}{s^4 + 88.5s^3 + 4.562x10^4s^2 + 9.376x10^5s + 2.585x10^4} \tag{3.11}$$

Table 3.4 Properties of the $G_{iP}(s)$

Zero of the transfer function	-0.028
Poles of the transfer function	-0.028, -21.19, -33.64±207.51i
Dc gain of the transfer function	$4.552x10^5$

Characteristic equation of $G_{iP}(s)$ is fourth order. An attempt is made to reduce the order of the function with keeping the location of the zero and two dominant poles together and having the same dc gain.

$$G_{red}(s) = \frac{9.634x10^6(s + 0.028)}{(s + 0.028)(s + 21.19)} \tag{3.12}$$

Time and frequency domain response comparison of $G_{iP}(s)$ and $G_{red}(s)$.

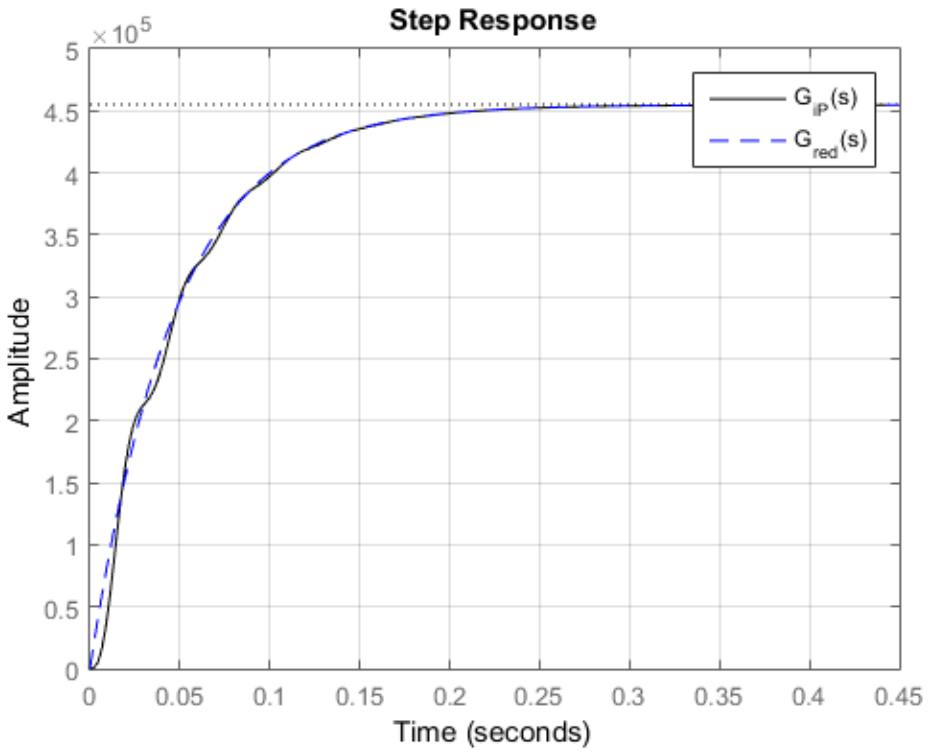

Figure 3.1. Step response of $G_{iP}(s)$ and $G_{red}(s)$

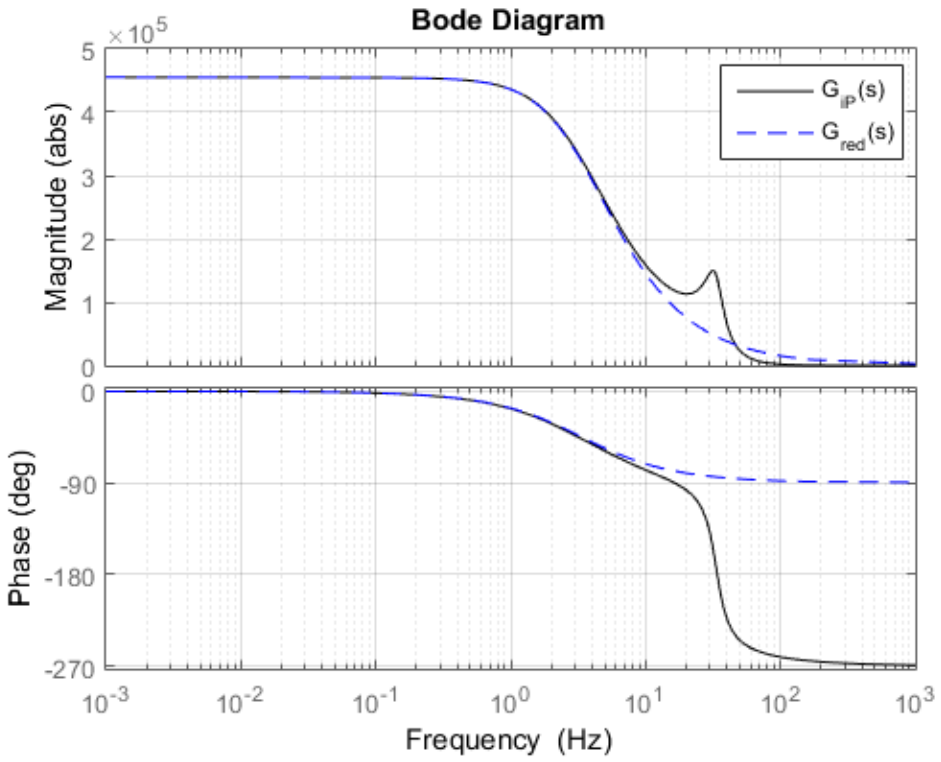

Figure 3.2. Bode plot of $G_{iP}(s)$ and $G_{red}(s)$

Agreement between $G_{iP}(s)$ and $G_{red}(s)$ is evident from the step response and bode plots. However, when the root locus plot of $G_{iP}(s)$ is inspected to see how poles of the closed loop system moves with increased controller gain, it is noticed that neglected pole pair rapidly moves towards the imaginary axis and becomes significant on the behaviour of the system.

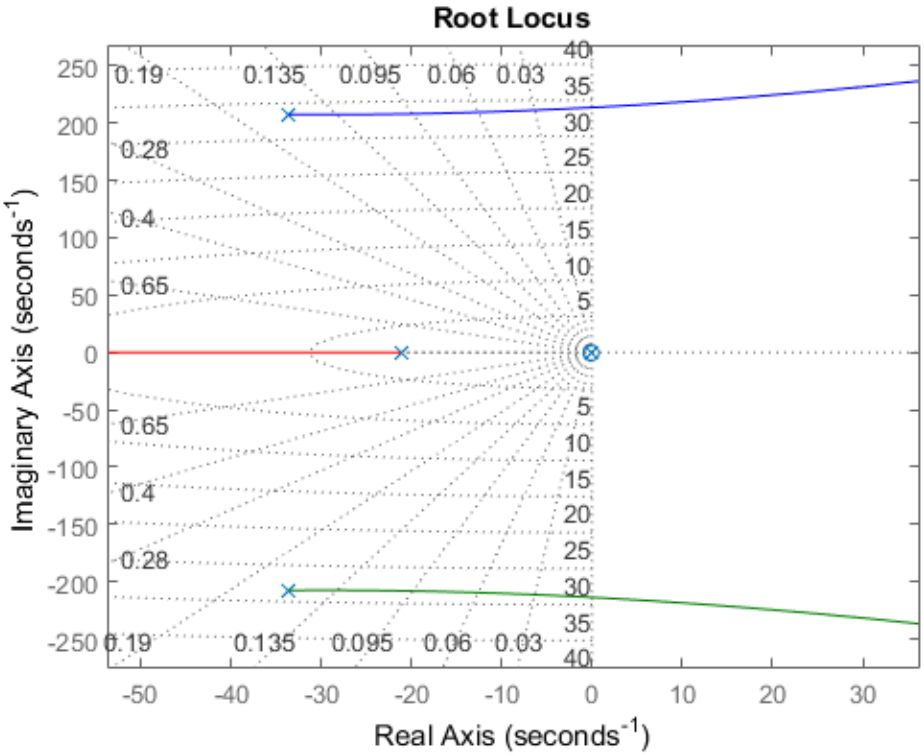

Figure 3.3. Root Locus of $G_{iP}(s)$

Hence, controller is directly designed using the 4^{th} order transfer function. Because of the challenging high order nature of the plant the well-known Ziegler-Nichols method which is a heuristic method of tuning PID controller is used.

Controller form is selected as:

$$G_{PIcont}(s) = \frac{K_p s + K_i}{s} \tag{3.13}$$

Firstly, ultimate gain, K_u, that makes the closed loop system marginally stable needs to be found. This can be directly found by the root locus plot. and verified by simulating the step response of the closed loop system. The gain when the pole pair at $-33.64 \pm 207.51i$ intersects with the imaginary axis is the ultimate gain and the period of limit cycle oscillations, T_u can be found again by the plot.

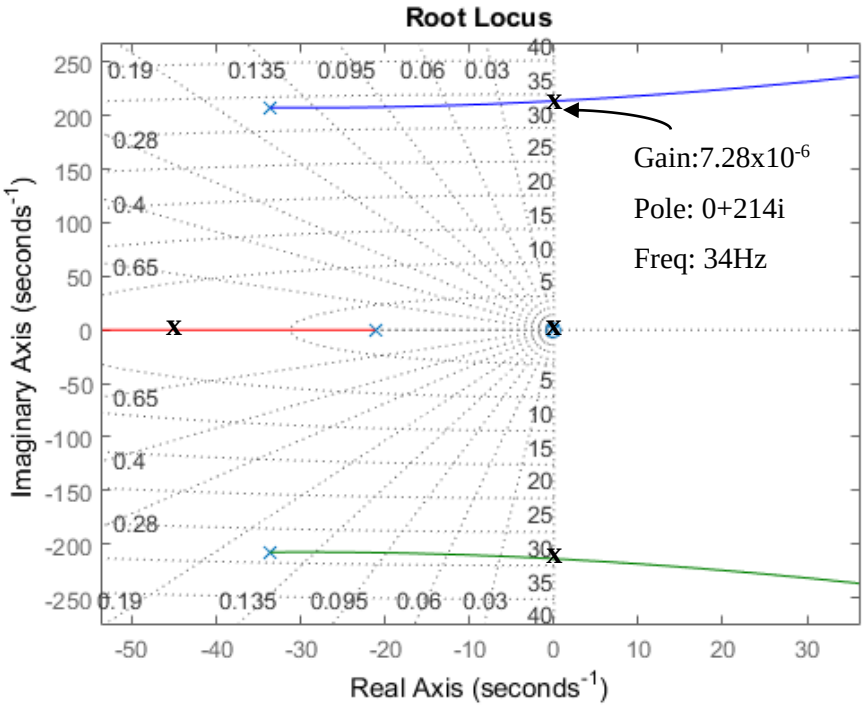

Figure 3.4. Ultimate Gain Pole Locations on Root Locus

For $K_u = 7.28 \times 10^{-6}$, limit cycle frequency is $34\ Hz$. Period of oscillation can be directly calculated as.

$$T_u = \frac{1}{34Hz} = 0.029sec \tag{3.14}$$

According to Ziegler-Nichols method controller gains can be calculated as follows:

$$K_p = 0.45K_u = 3.276x10^{-6} \tag{3.15}$$

$$K_i = 0.54K_u/T_u = 1.337x10^{-4} \tag{3.16}$$

Closed loop transfer function with selected controller gains is:

$$G_{cl}(s) = \frac{G_{iP}(s)G_{PIcont}(s)}{1 + G_{iP}(s)G_{PIcont}(s)} = \frac{1.40x10^6s^2 + 5.70x10^7s + 1.57x10^6}{s^5 + 88.5s^4 + 4.56x10^4s^3 + 2.33x10^6s^2 + 5.70x10^7s + 1.57x10^6} \tag{3.17}$$

Step response of the $G_{cl}(s)$:

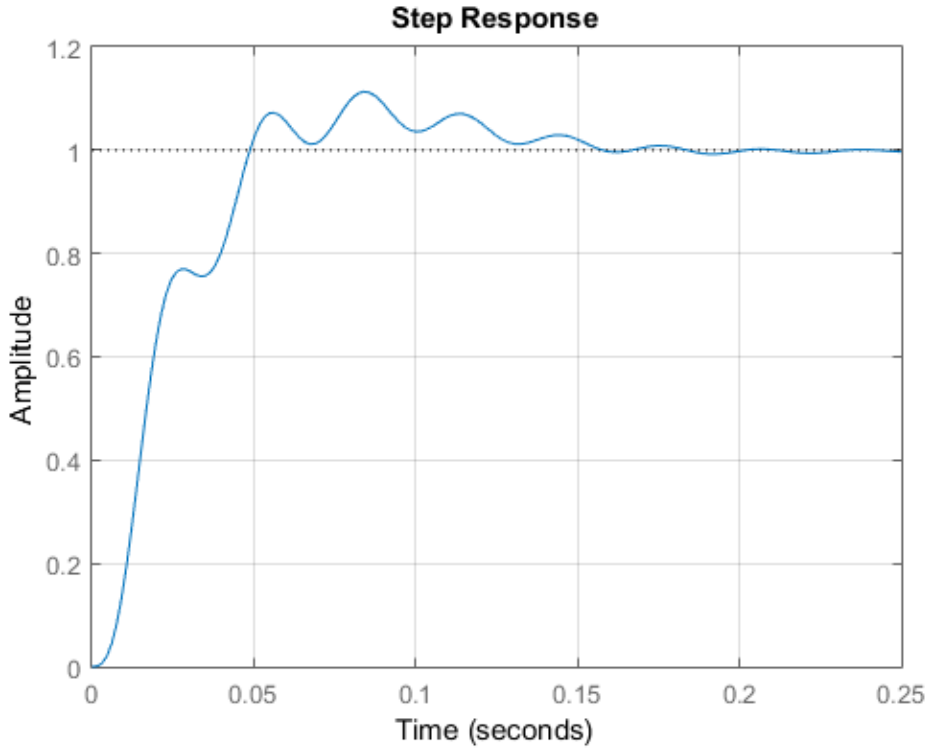

Figure 3.5. Step response of $G_{cl}(s)$

Step response of the closed loop system has 11% overshoot and its rise time and settling time are 0.04 sec and0.15 sec, respectively. This is a satisfactory result for the linearization point. Even though transient characteristics might change for other operational points, system is expected to behave stable.

Controllers work in a discrete environment, thus designed controller needs to be discretised. There are three common ways to discretise the continuous transfer function, those are forward Euler, backward Euler and Tustin method. To discretise the designed the controller, backward Euler method is used. Variable s that appears in the transfer function of the controller is replaced with:

$$s = \frac{z-1}{z\,T_s} = \frac{1-z^{-1}}{T_s} \tag{3.18}$$

With the replacement shown in equation (3.18), $G_{PIcont}(s)$ can be written in discrete form:

$$G_{PIcont,disc}(z) = K_p + K_i T_s \frac{z}{z-1} \tag{3.19}$$

In equation (3.18), T_s is the sampling time which is set as $0.001s$. After discretization, discretised controller becomes:

$$G_{PIcont,disc}(z) = 3.276x10^{-6} + 1.337x10^{-7} \frac{z}{z-1} \tag{3.20}$$

For the simplified linear and linear close loop model simulations that are presented in chapter 4, discretised PI controller is used.

3.4.2 Controller Design with Nonlinear Model

Simulation results of the nonlinear model with the controller designed in the section 3.4.1 leads limit cycle in outlet pressure. Two simplifications were used to simplify the nonlinear model into simplified nonlinear model. And oscillations on the outlet pressure is not observed on the simplified nonlinear model. Hence, root cause of the oscillation is related with the simplifications. By setting magnitude of the coulomb friction force in the nonlinear model to zero, friction force is eliminated, and simulation are run to see the effect of coulomb friction on the nonlinear model of the hybrid pressure regulator. The results can be seen in Figure 3.6. Cause of the oscillations is the controller's poor performance in the existence of coulomb friction and stick-slip effect that the friction creates.

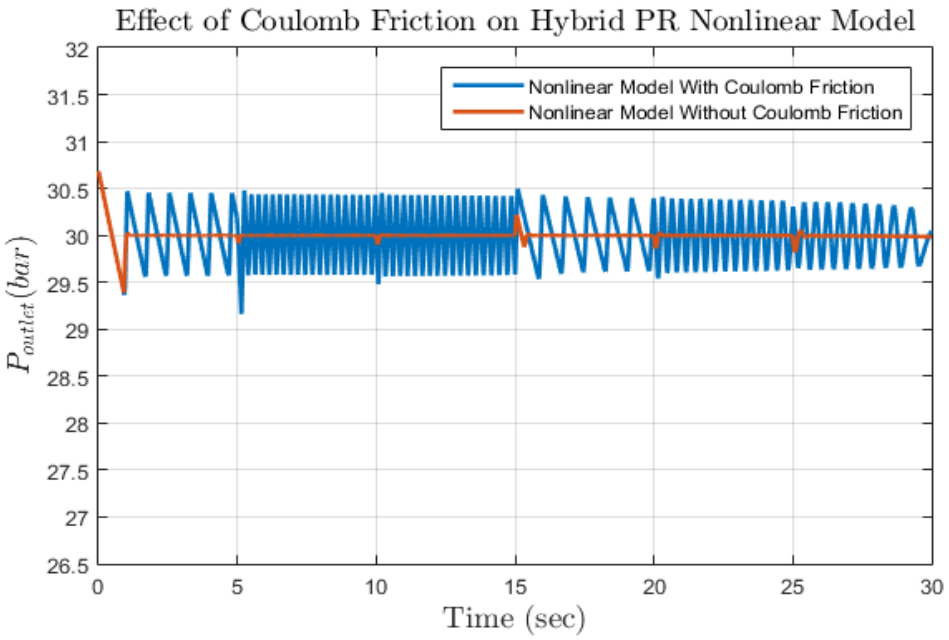

Figure 3.6. Effect of Coulomb Friction on Hybrid PR Nonlinear Model

Limit cycle magnitude is directly related with the magnitude of the friction. Simulation result of nonlinear model with PI controller and mentioned limit cycle are shown in figure below.

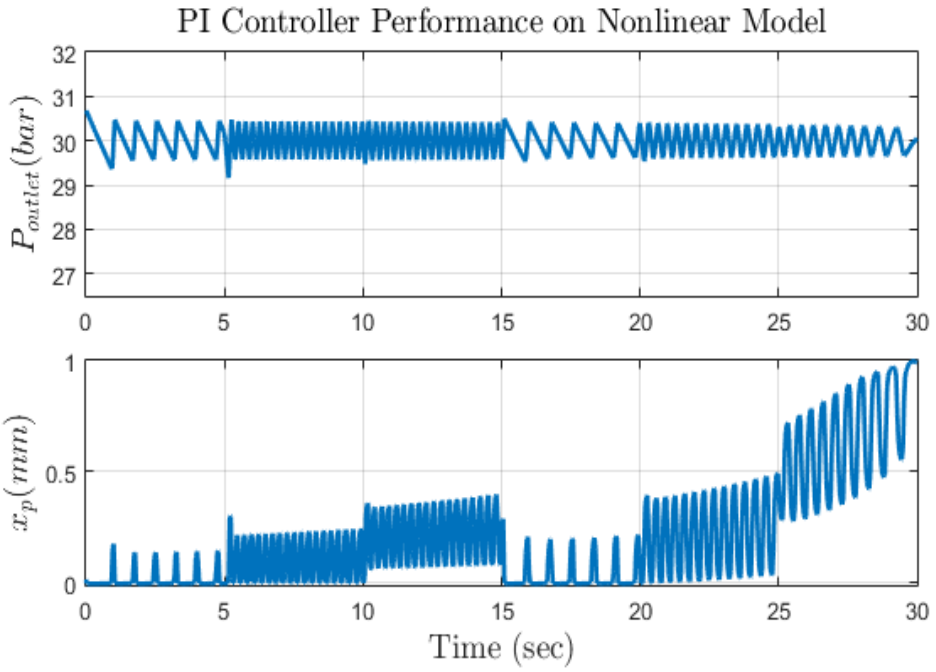

Figure 3.7. PI Controller Performance on Nonlinear Model

Thus, PID controller with derivative filter is designed directly for the nonlinear model utilizing the PID Tuner of Matlab Simulink.

Designed controller has the following form in discrete domain:

$$G_{PIDcont\_disc} = K_p + K_i T_s \frac{z}{z-1} + K_d \frac{N}{1 + N\, T_s \frac{z}{z-1}} \tag{3.21}$$

Derivative filter coefficient, N, is selected as low as possible, since main aim of the controller is to eliminate the steady state error, rather than improving transient characteristics. Hence, filter cut-off frequency is selected as $5Hz$. Parameters of the $G_{PIDcont\_disc}$ is selected as:

$$\begin{gathered} K_p = 9.772x10^{-6}, \qquad K_i = 1.764x10^{-5}, \qquad K_d = 2.685x10^{-5}, \\ N = \quad 31.416, \qquad T_s = 0.001 \end{gathered} \tag{3.22}$$

Plugging in equation (3.22) into equation (3.21) yields the following controller:

$$G_{PIDcont\_disc} = 9.77x10^{-6} + 1.76x10^{-8} \frac{z}{z-1} + \frac{8.43x10^{-6}}{1 + 0.031 \frac{z}{z-1}} \tag{3.23}$$

Designed discrete PID controller stabilizes the nonlinear model for the conditions that are defined as the operational envelope. For the nonlinear close loop model simulations that are presented in chapter 4, discrete PID controller is used.

CHAPTER 4

SIMULATION RESULTS

Hybrid pressure regulator is simulated with its nonlinear, simplified nonlinear and linearized model to compare their results. During simulations plant model is simulated in continous form however controller is run in a discrete time domain with a sampling time of $0.001s$ $(i.e\ 1000Hz)$. For simplified nonlinear and linearized models the discrete PI controller designed in section 3.4.1 is used, whereas for the nonlinear model the discrete PID controller designed in section 3.4.2 is used.

Each hybrid pressure regulator model is run with four different mass flow rate conditions with the same inlet pressure and temperature profile and their results are compared with mechanical pressure regulator model which has the same design parameters but without actuation mecahnism and voice coil actuator. Thus, only difference between the hybrid pressure regulator and mechanical pressure regulator apart from the control action, is the change of equivelant mass, m_{eq}. For the mechanical pressure regulator model equivelant mass is the combination of poppet, piston, and effective spring mass which equals to $231g$.

Also, to showcase the robustness of the designed hybrid pressure regulator, power loss is introduced during operation. Power loss is simulated by setting the voice coil current to zero.

4.1 Simulation Scenario

Conditions of high-pressure inlet helium tank is started from $300bar$ and $330°K$ and decreased down to $60bar$ and $230°K$ in $30s$ as the helium consumed by various flow lines. During this period pressure regulator should operate and control pressure of its downstream where on/off solenoid valves of the cold gas thruster system are

located for spacecraft`s attitude control system. Depending on the number of valves that needs to be opened simultaneously, mass flow rate demand can be switched between $10g/s$, $50g/s$ and $90g/s$.

Inlet pressure and temperature profile is shown below:

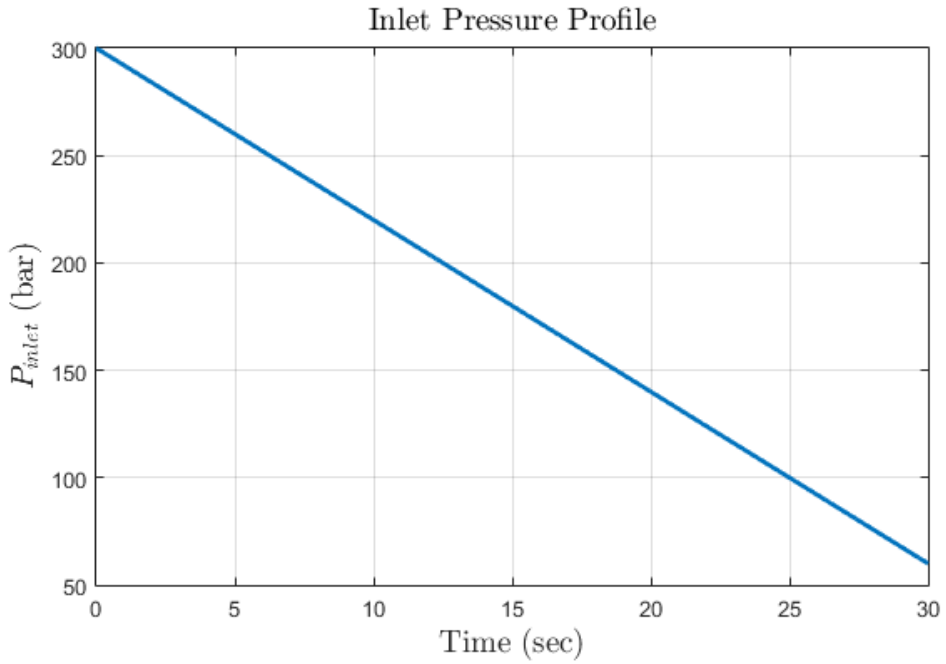

Figure 4.1. Inlet Pressure Profile

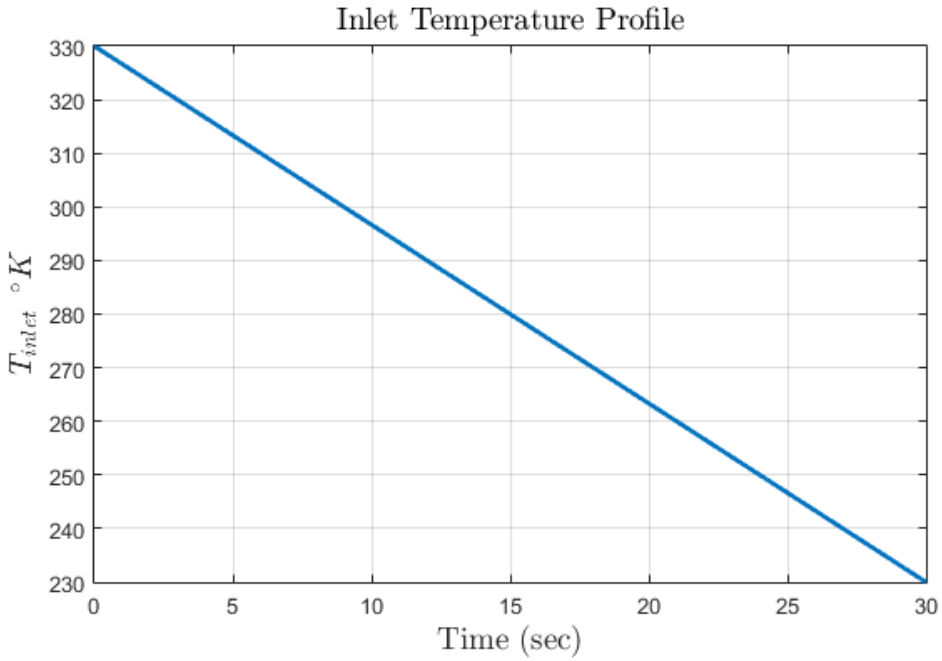

Figure 4.2. Inlet Temperature Profile

4.2 Depressurization with Constant Mass Flow Rate Demand

Separate simulations are run for different mass flow rate demands with fixed consumption at $10g/s, 50g/s$ and $90g/s$.

Simulations of mechanical pressure regulator nonlinear model, simplified nonlinear model and linearized model are run to have a base rating for pressure regulation performance. Results are shown from Figure 4.3 to Figure 4.5.

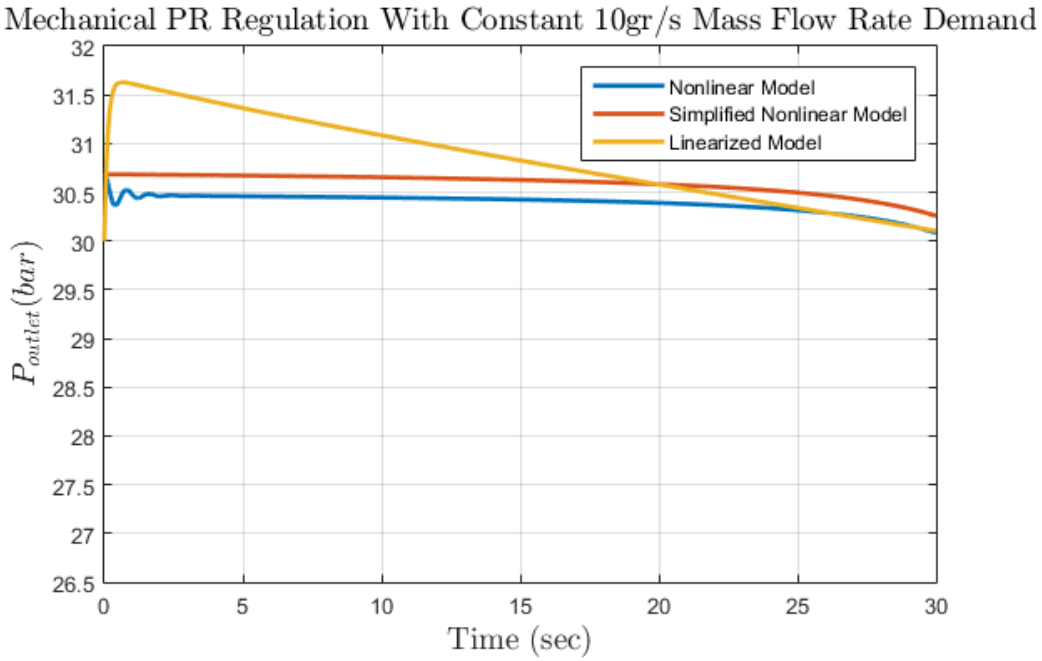

Figure 4.3. Mechanical PR Regulation with Constant 10gr/s Mass Flow Rate Demand

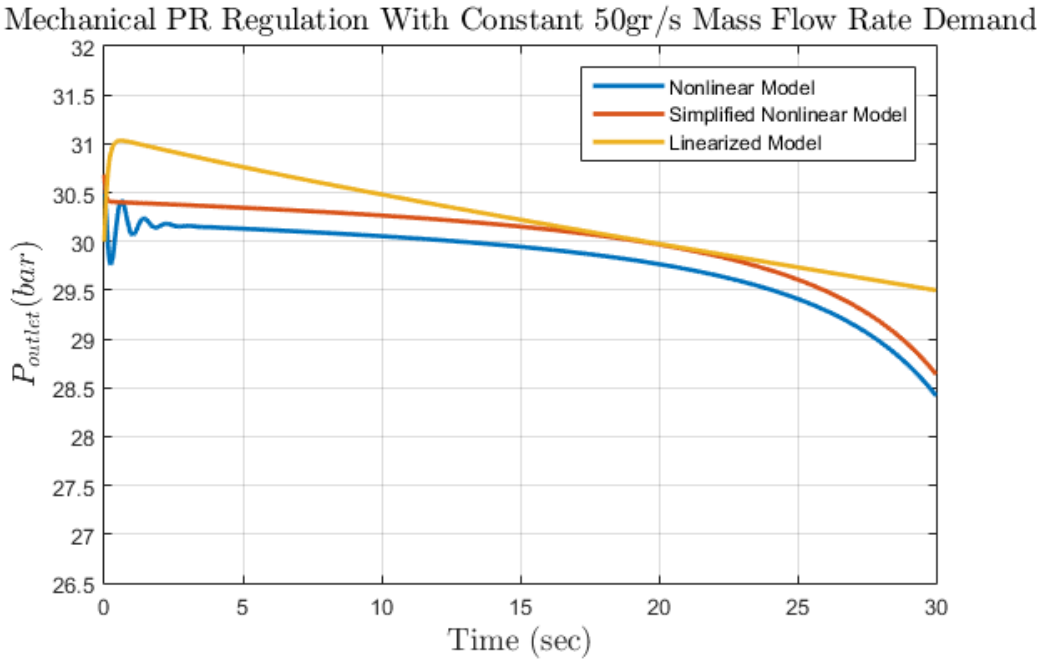

Figure 4.4. Mechanical PR Regulation with Constant 50gr/s Mass Flow Rate Demand

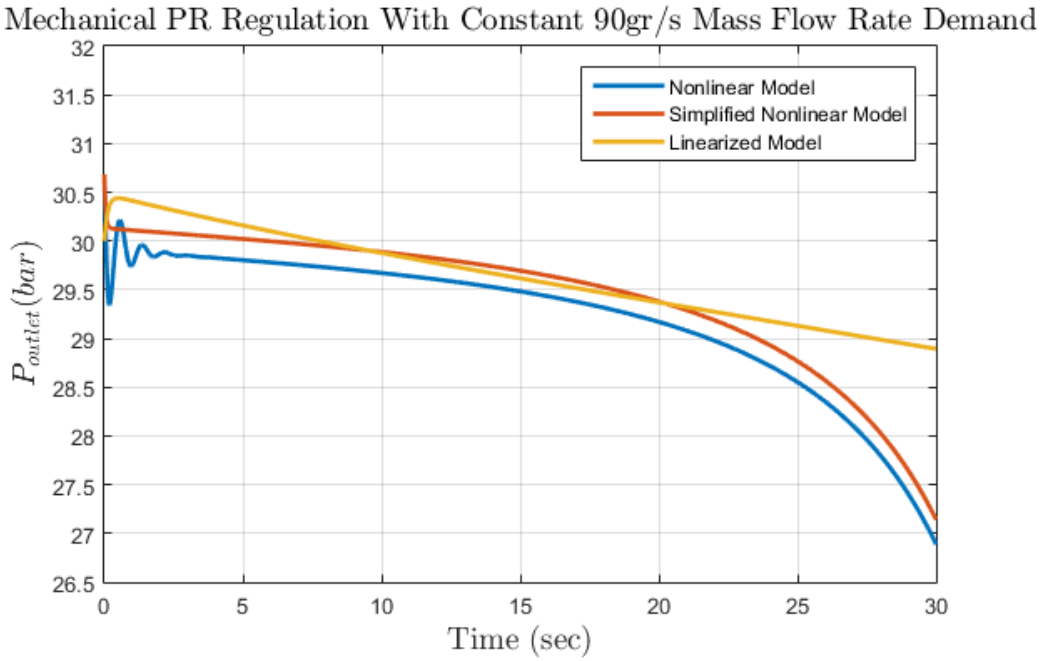

Figure 4.5. Mechanical PR Regulation with Constant 90gr/s Mass Flow Rate Demand

As seen in Figure 4.3, Figure 4.4 and Figure 4.5 linearized model has good agreement with the simplified nonlinear model as around its linearization point. However, as we move away from the linearization point (i.e., start and end of the simulation), nonlinear effects get stronger, and results starts to differ as expected.

Also, there is good correlation between the nonlinear model and simplified nonlinear model throughout the whole simulation. Apparent, constant gap between settled responses is mainly caused by the modelled coulomb friction which is excluded from the model during simplification process.

Besides, the outlet pressure, poppet positions can be inspected as well:

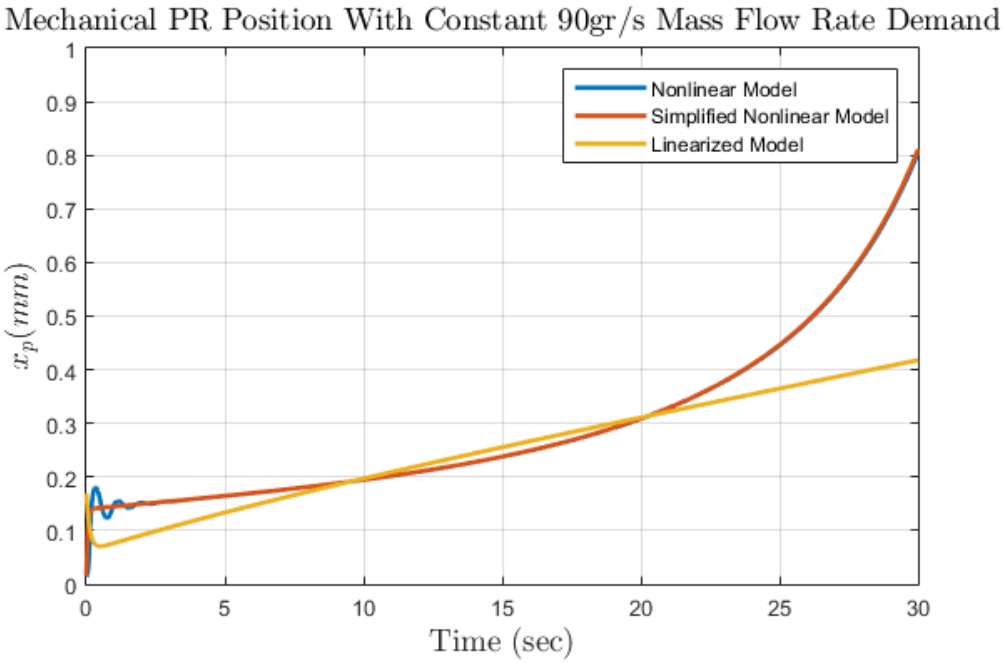

Figure 4.6. Mechanical PR Position with Constant 90gr/s Mass Flow Rate Demand

Position of the moving assembly is shown in Figure 4.6 for the constant $90gr/s$ mass flow rate demand case which also supports the abovementioned comments.

Simulations of hybrid pressure regulator non-linear model, simplified non-linear model and linearized model are run. Results are shown from Figure 4.7 to Figure 4.9.

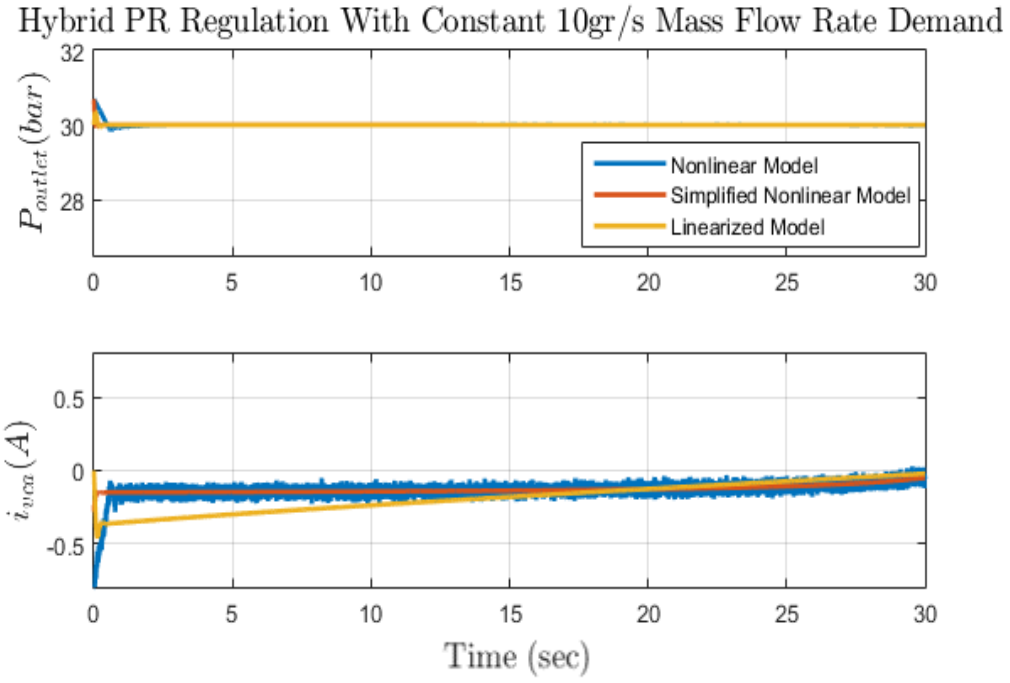

Figure 4.7. Hybrid PR Regulation With Constant 10gr/s Mass Flow Rate Demand

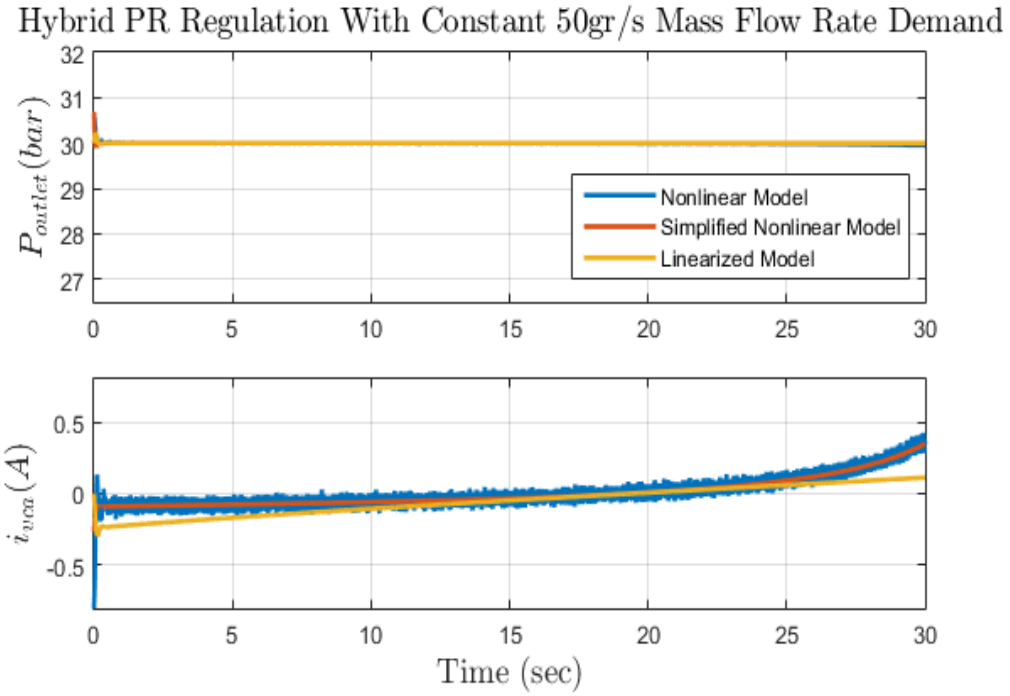

Figure 4.8. Hybrid PR Regulation With Constant 50gr/s Mass Flow Rate Demand

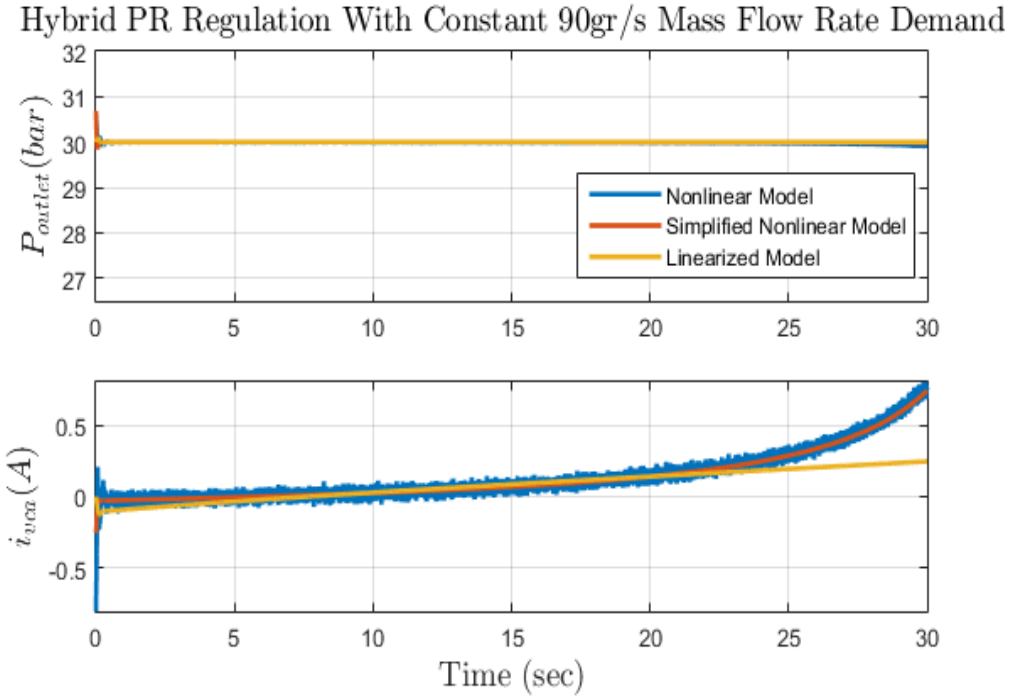

Figure 4.9. Hybrid PR Regulation With Constant 90gr/s Mass Flow Rate Demand

Control effort to regulate the outlet pressure to the desired set pressure can be seen in Figure 4.7, Figure 4.8 and Figure 4.9. For $10gr/s$, $50gr/s$ and $90gr/s$ constant flow rate conditions, each pressure regulator model displayed an increase in the regulation performance.

Performance and error comparison of mechanical pressure regulator and hybrid pressure regulator are displayed in Figure 4.10 and Figure 4.11.

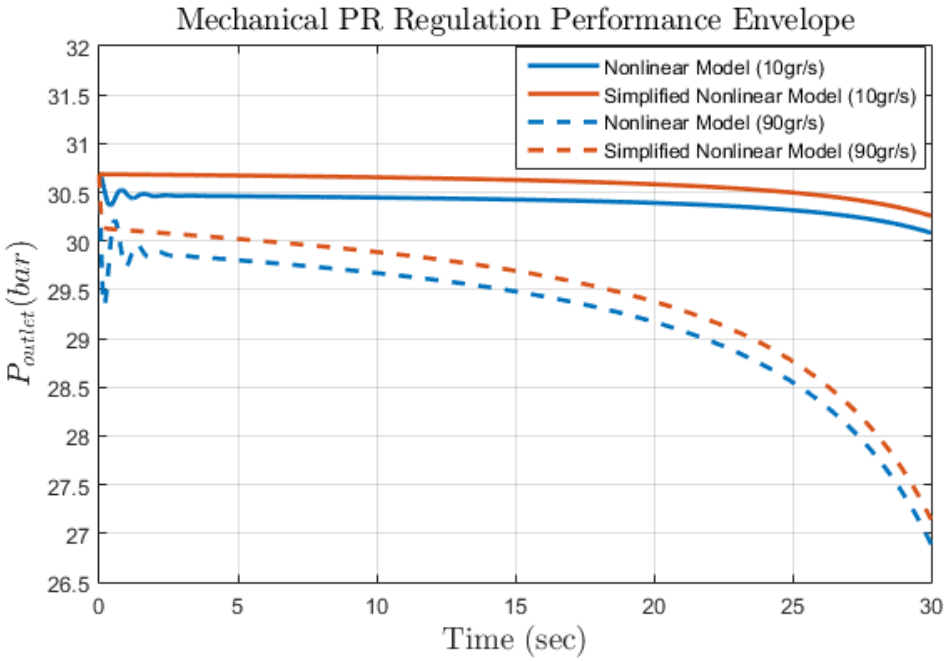

Figure 4.10. Mechanical PR Regulation Envelope

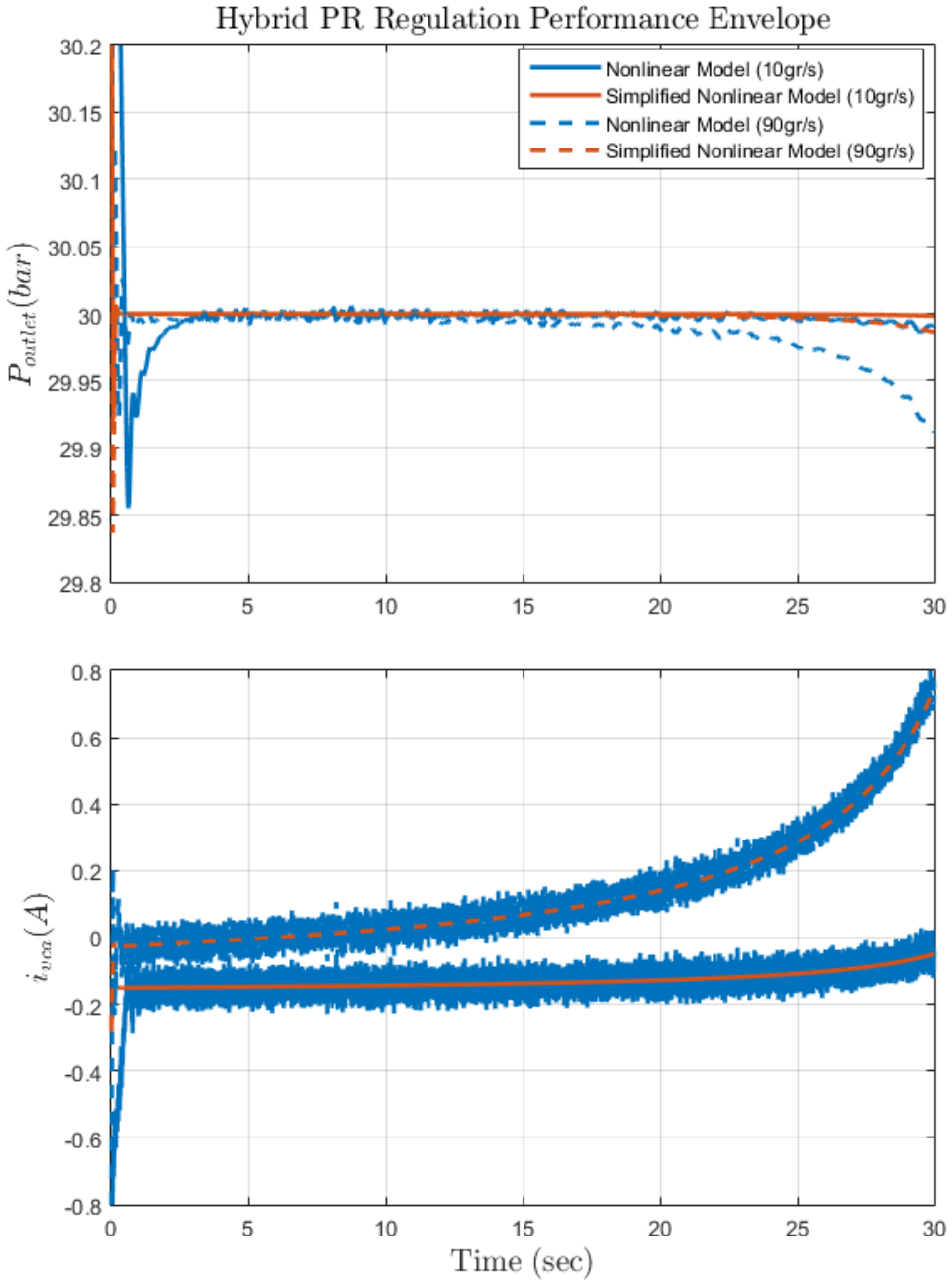

Figure 4.11. Hybrid PR Regulation Envelope

As seen, pressure regulation performance of the hybrid pressure regulator is greatly higher than the classic mechanical pressure regulator, thanks to active control of voice coil.

Also, power loss scenario is inspected to demonstrate the fault tolerance of the proposed hybrid pressure regulator. Power loss is introduced at $t = 15s$ by setting the voice coil current to 0 for the hybrid pressure regulator.

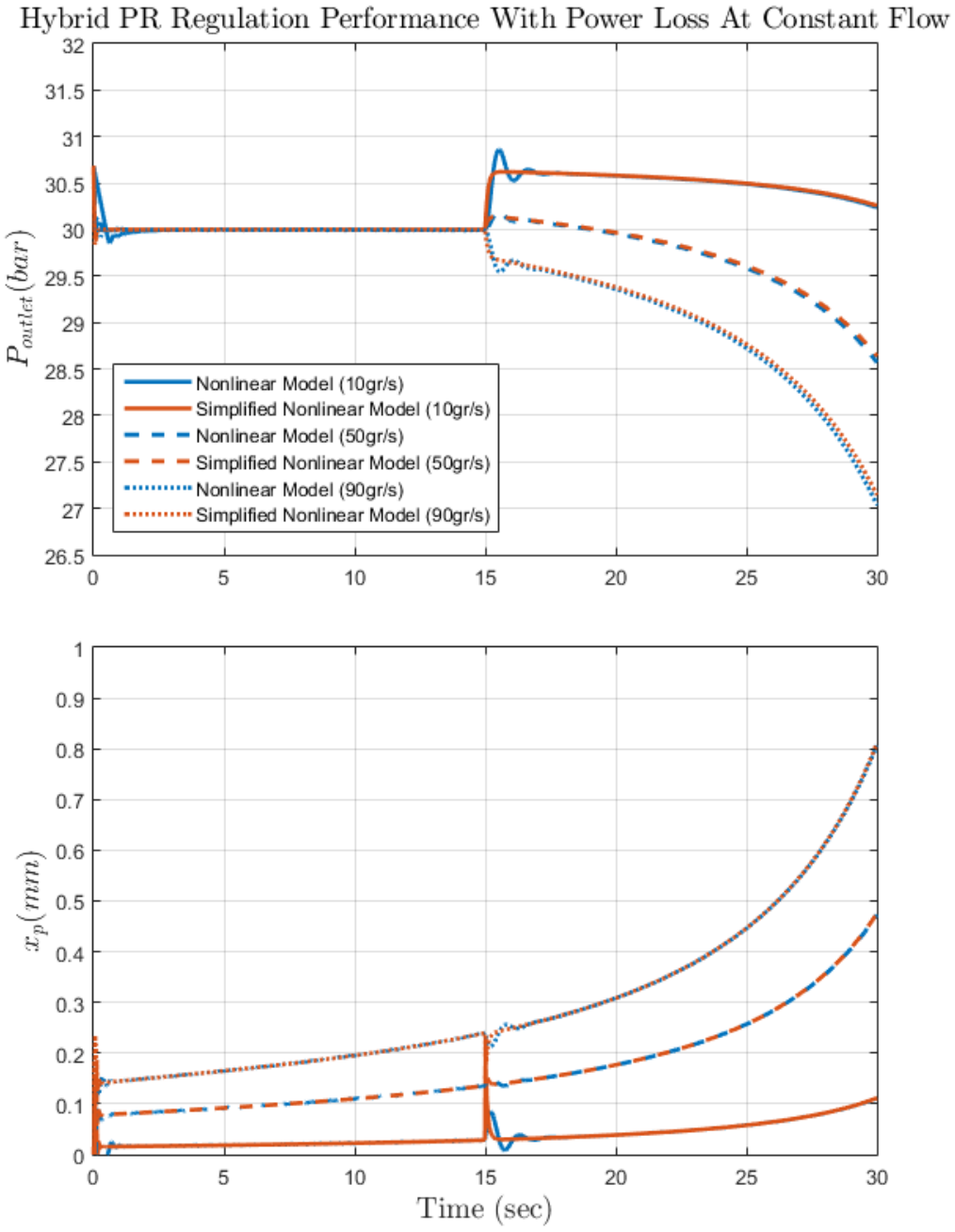

Figure 4.12. Hybrid PR Regulation Performance With Power Loss At Constant Flow

As seen from Figure 4.12, after power loss, hybrid pressure regulator behaves as a mechanical pressure regulator. Hence, pressure regulation performance is degraded but still maintained.

4.3 Depressurization with Changing Mass Flow Rate Demand

Mass flow rate demand is switched sin every five seconds between $10g/s, 50g/s$ and $90g/s$. Varying mass flow rate demand is shown in Figure 4.13:

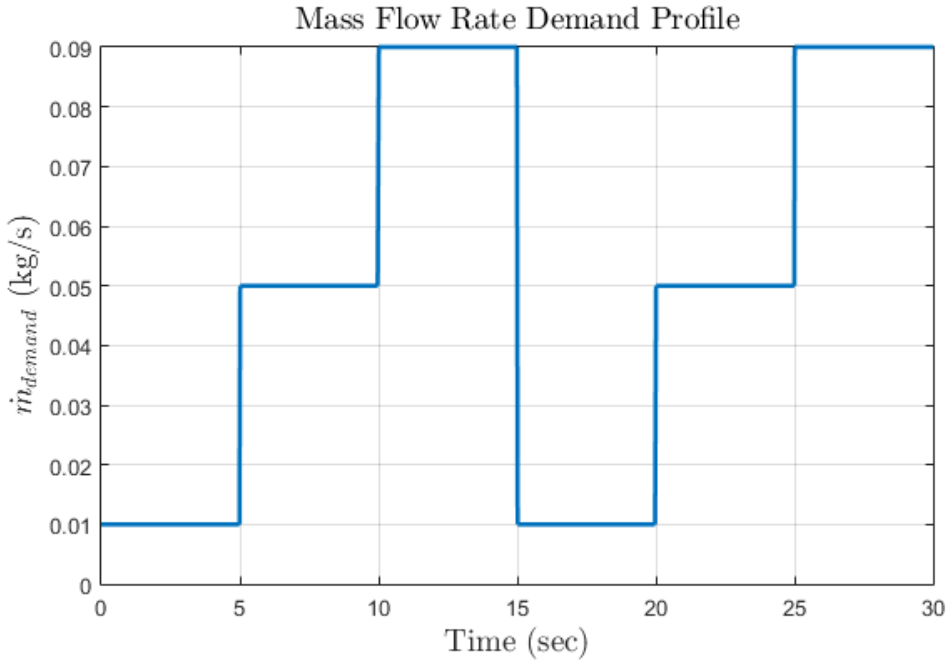

Figure 4.13. Varying Mass Flow Rate Demand Profile

Simulations of mechanical pressure regulator nonlinear model, simplified nonlinear model and linearized model are run to have a base rating for pressure regulation performance. Results are shown in Figure 4.14.

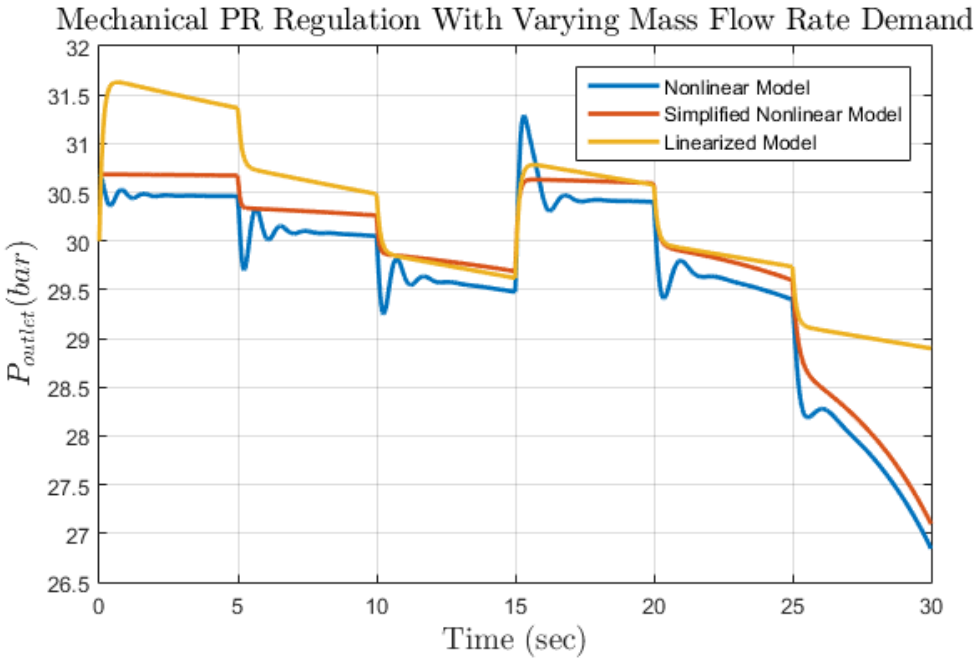

Figure 4.14. Mechanical PR Regulation with Varying Mass Flow Rate Demand

The reason of apparent transient characteristics difference and constant gap between settled responses is mainly caused by the coulomb friction in nonlinear model.

Simulations of hybrid pressure regulator non-linear model, simplified non-linear model and linearized model are run. Results are shown in Figure 4.15 and Figure 4.16.

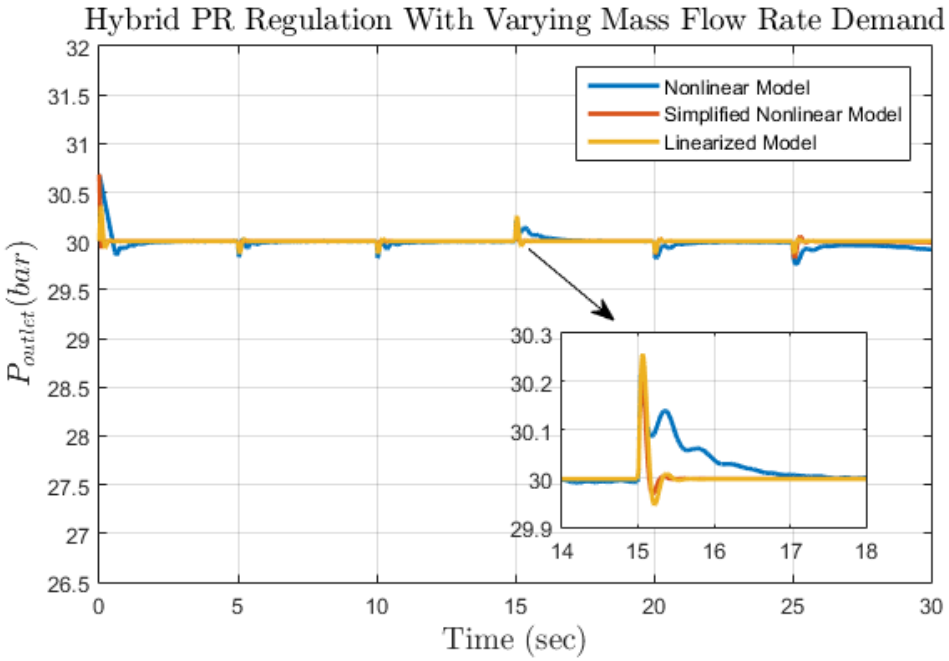

Figure 4.15. Hybrid PR Regulation with Varying Mass Flow Rate Demand

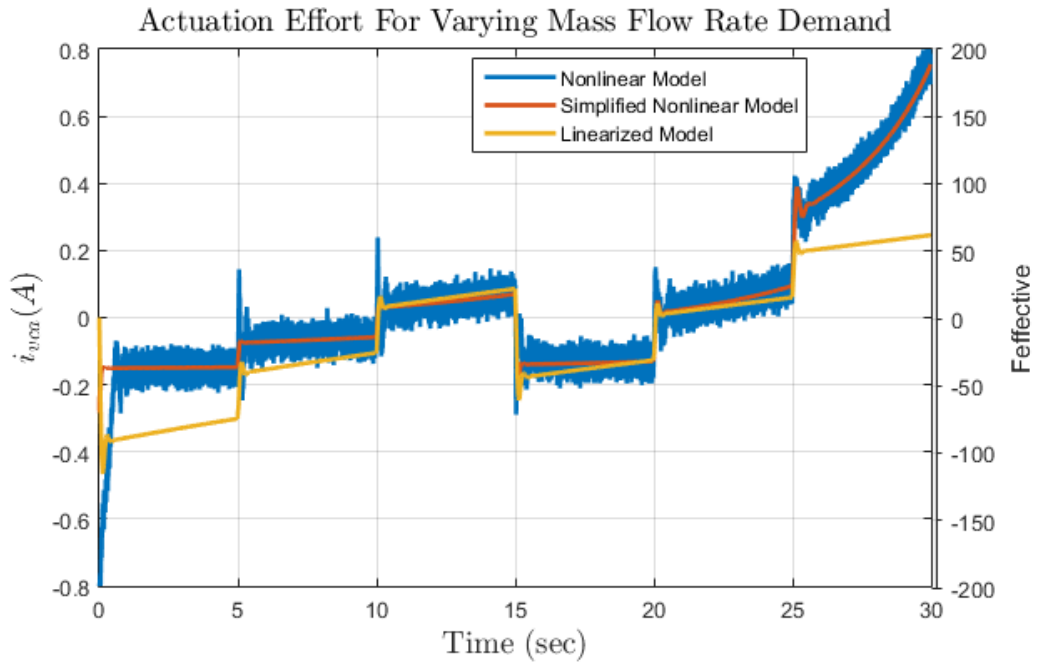

Figure 4.16. Actuation Effort During Varying Mass Flow Rate

As seen, even with varying mass flow rate demand, hybrid pressure regulator quickly regulates the outlet pressure to its desired set pressure level. Used control effort and its effective force on the piston-poppet assembly is shown in Figure 4.16.

Also, power loss scenario is inspected to demonstrate the fault tolerance of the proposed hybrid pressure regulator. Power loss is introduced at $t = 15s$ by setting the voice coil current to 0 for the hybrid pressure regulator.

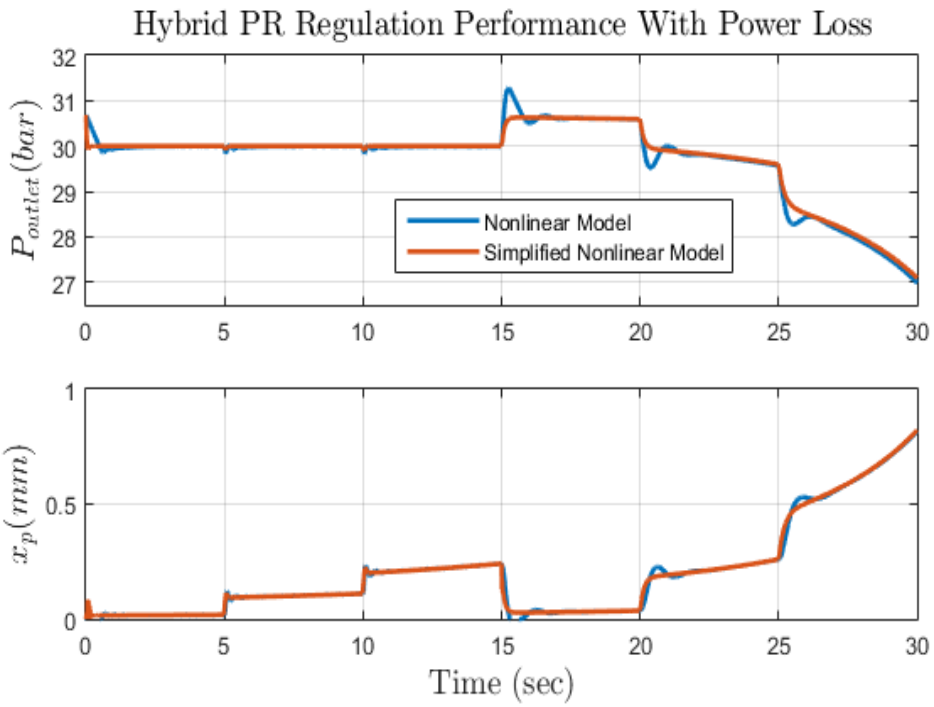

Figure 4.17. Hybrid PR Regulation Performance With Power Loss

As seen in Figure 4.17, hybrid pressure regulator behaves as a mechanical pressure regulator after the power loss and it keeps the outlet pressure regulated with a degraded regulation performance.

CHAPTER 5

CONCLUSION

In this study, modelling, control and simulation of novel hybrid pressure regulator design is studied, coupling of voice coil actuator to pressure regulator is explained. In this respect, detailed nonlinear mathematical model of hybrid pressure regulator is formed by utilizing governing equations, then this model is simplified to achieve continous nonlinear model, which is referred as simplified nonlinear model. Simplified nonlinear model is then linearized around an operating point to achieve a linearized model of the hybrid pressure regulator.

Hypotetical but realistic operational envelope of the pressure regulator is defined and parameters of the regulator are chosen according to specified values. Linearized model is calculated by chosen parameter and operating point. Two controllers are designed. PI controller is used for linearized and simplified nonlinear model wheras PID controller is used for the nonlinear model.

Simulation scenario is set in compliance with the predefined operational envelope. Mechanical pressure regulator model is created from the hybrid pressure regulator model by discarding the actuator mechanism to have a baseline for the pressure control performace. Then, hybrid pressure regulator performance is evaluated against the mechanical pressure regulator for constant and varying mass flow rate demand conditions. Advantages of the proposed hybrid pressure regulator model is observed over the mechanical pressure regulator from simulations.

Additionally, robustness of the hybrid pressure regulator against power loss is also simulated. It is observed that, eventhough the regulation performance degrades with the loss of voice coil actuator, hybrid pressure regulator keeps regulating like a traditional mechanical pressure regulator.

To conclude, in this thesis it is shown with simulations that proposed hybrid pressure regulator design is capable of achieving high pressure regulation accuracy with a controlled voice coil actuator, at the same time it is fault tolerant in case of power loss. It can be used in both as laboratory equipment and space applications where high pressure accuracy is important and any failure in pressure regulation may lead high cost damage.

For future work, sensor and actuation dynamics can be added to the model. Also, proposed pressure regulator can be built and tested to verify the mathematical model, and controller can be tuned on the fly with tests.

REFERENCES

[1] F. Ning, Y. Shi, M. Cai, Y. Wang, and W. Xu, "Research progress of related technologies of electric-pneumatic pressure proportional valves," *Appl. Sci.*, vol. 7, no. 10, pp. 1–15, 2017.

[2] N. Zafer and G. R. Luecke, "Stability of gas pressure regulators," *Appl. Math. Model.*, vol. 32, no. 1, pp. 61–82, 2008.

[3] R. Mooney, "Pilot-Loaded Regulator: What You Need to Know," in *Gas Industries*, 1989, pp. 31–33.

[4] R. Brasilow, "The Basics of Gas Regulators," in *Welding Design and Fabrication*, 1989, pp. 61–65.

[5] A. Krigman, "Guide to selecting pressure regulators," in *InTech*, 1984, pp. 51–65.

[6] E. Gill, "Air-loaded regulators, the smart control valve alternative," in *InTech*, 1990, pp. 21–22.

[7] D. H. Tsai and E. C. Cassidy, "Dynamic behavior of a simple pneumatic pressure reducer," *J. Fluids Eng. Trans. ASME*, vol. 83, no. 2, pp. 253–264, 1961.

[8] A. Nabi and J. Dayan, "Dynamic model for a dome-loaded pressure regulator," *J. Dyn. Syst. Meas. Control. Trans. ASME*, vol. 122, no. 2, pp. 290–297, 2000.

[9] M. Avram, M. F. Tefănescu, A. Erban, A. Dobrovicescu, and B. Grămescu, "Analysis of a proportional pressure regulator," in *IOP Conference Series: Materials Science and Engineering*, 2019, vol. 595, no. 1.

[10] B. K. Saha, "Numerical Simulation of a Pressure Regulated Valve to Find Out the Characteristics of Passive Control Circuit," *Int. J. Mech. Mechatronics*

Eng., vol. 7, no. 5, pp. 936–939, 2013.

[11] D. J. Kukulka, A. Benzoni, and J. C. Mollendorf, "Digital Simulation of a Pneumatic Pressure Regulator," *Simulation*, vol. 63, no. 4, pp. 252–266, 1994.

[12] M. Ramzan and A. Maqsood, "Dynamic Modeling and Analysis of a High Pressure Regulator," *Mathematical Problems in Engineering*, vol. 2016. 2016.

[13] J. Unde, "Simulating ' Electronic Pressure Regulator ' using MATLAB Simulink," pp. 1–6, 2018.

[14] G. P. Jayaraman and S. V. Lunzman, "An observer design for a poppet type pressure reducing valve," *Proc. IEEE Int. Conf. Control Appl.*, pp. 76–81, 2011.

[15] A. A. Shaalan, M. F. Badr, and E. S. Al-Ameen, "Motion control of electro-pneumatic system based on directional control solenoid valve," *Int. J. Mech. Prod. Eng. Res. Dev.*, vol. 9, no. 2, pp. 211–222, Apr. 2019.

[16] A. Nabi, "The Dynamics of Fast Responding Dome-Loaded Pressure Regulator," Haifa Technion, 1986.

[17] B. W. Anderson, *The Analysis and Design of Pneumatic Systems*. New York: Wiley, 1967.

[18] J. A. Perry, *Critical Flow through Sharp-edged Orifices*. Trans. ASME, 1949.

[19] H. Fleischer, *Manual of Pneumatic System Operation*. New York, NY, USA: McGraw-Hill, 1995.

[20] J. Reid and C. D. Stewart, "A review of critical flow nozzles for the mass flow measurement of gases," in *2nd International Symposium on Fluid Control Measurement Mechanics and Flow Visualization*, pp. 454–457.

[21] Z. Mozer, A. Tajti, and V. Szente, "Experimental investigation on pneumatic components," *12th Int. Conf. Fluid Flow Technol.*, pp. 517–524, 2003.

[22] A. R. Shahani, A. Aryaei, H. Esmaili, M. Najar, and S. Mohammadi, “Mathematical modeling of a high pressure regulator with safety valve,” in *ASME 2010 10th Biennial Conference on Engineering Systems Design and Analysis, ESDA2010*, 2010, vol. 5, pp. 457–463.

[23] I. Newton, *Mathematical Principles of Natural Philosophy*. Berkeley: University of California Press, 1729.

[24] A. Sharma, “Newton ’ s generalized form of second law gives F = ma,” *J. Appl. Phys.*, vol. 13, no. 2, pp. 61–137, 2021.

[25] L. Ruby, “Equivalent mass of a coil spring,” *Phys. Teach.*, vol. 38, no. 3, pp. 140–141, 2000.

[26] E. Meriläinen, “Current-driving of loudspeakers: Remedy to the fundamental fallacy of sound reproduction technology.” 2009.

[27] Y. M. Choi and D. G. Gweon, “A high-precision dual-servo stage using halbach linear active magnetic bearings,” *IEEE/ASME Trans. Mechatronics*, vol. 16, no. 5, pp. 925–931, 2011.

[28] P. G. L. Mills and M. O. J. Hawksford, “Distortion reduction in moving-coil loudspeaker systems using current-drive technology,” *AES J. Audio Eng. Soc.*, vol. 37, no. 3, pp. 129–148, 1989.

[29] E. Sturtzer, G. Pillonnet, G. Lemarquand, and N. Abouchi, “Comparison between voltage and current driving methods of a micro-speaker,” *Appl. Acoust.*, vol. 73, no. 11, pp. 1087–1098, 2012.

[30] W. McMahan and K. J. Kuchenbecker, “Dynamic modeling and control of voice-coil actuators for high-fidelity display of haptic vibrations,” *IEEE Haptics Symp. HAPTICS*, no. February 2014, pp. 115–122, 2014.

APPENDICES

A. Seal Friction Parameter Estimation

The magnitude of friction force of a reciprocating o-ring depends on several factors. Some of those factors are; pressure magnitude, size, material, hardness and squeeze of the o-ring, mating surface roughness, use of lubrication and temperature. Therefore, it is not practical to have a generalized formula to calculate the magnitude of seal friction with that many factors in it. Thankfully, there are results of experimental studies that are published by Parker® to give us engineers an estimation of the magnitude of friction.

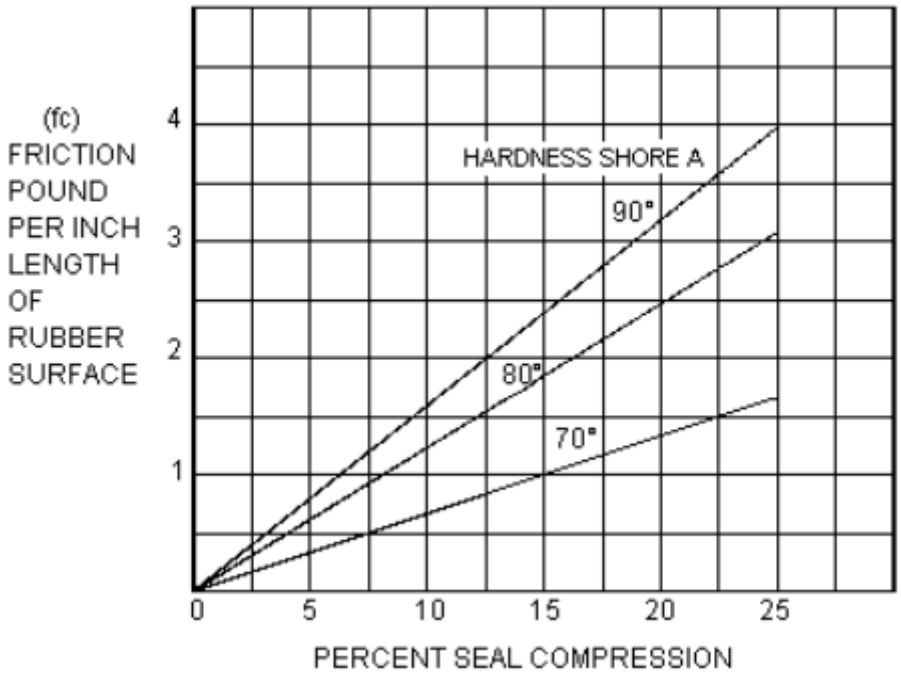

Figure 5.1. O-Ring Friction fc Factor Estimation

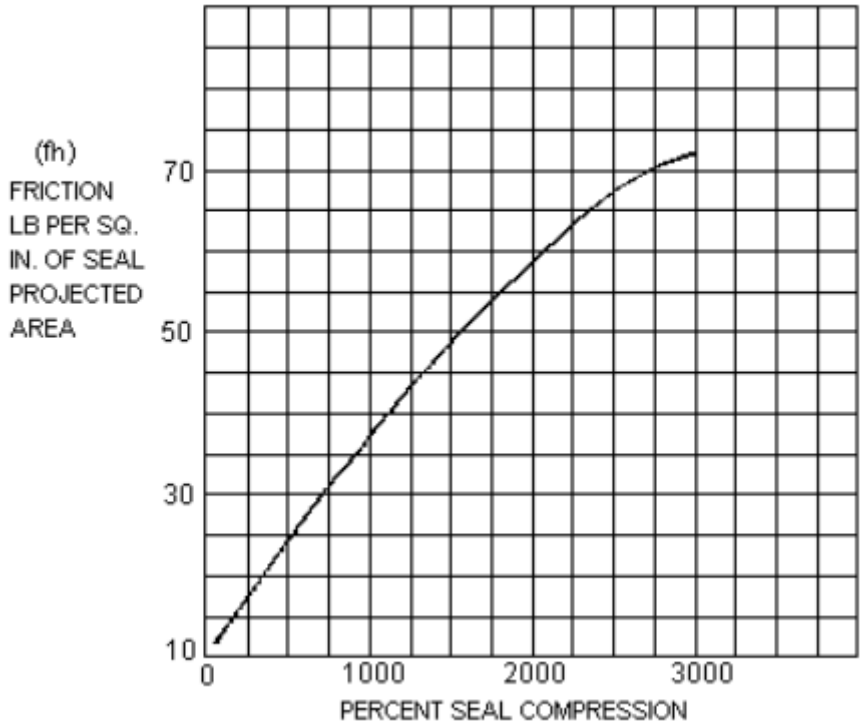

Figure 5.2. O-Ring Friction fh Factor Estimation

Note that in Figure 5.2, original source has a typo on x-axis label which supposed to be Pressure in Psi.

Estimating friction for piston groove and rod groove are given separately as:

$$F_{coul,piston} = (fc_{piston})(L_p) + (fh_{piston})(A_p) \quad (5.1)$$

$$F_{coul,rod} = (fc_{rod})(L_r) + (fh_{rod})(A_r) \quad (5.2)$$

In equation (5.1) (5.2); L_p and L_r are lengths of rubbing surfaces of piston ad rod seals respectively. Similarly, A_p and A_r are projected areas of rubbing surfaces of piston ad rod seals respectively.

For the modelled hybrid pressure regulator parameters that is used for estimating friction magnitude is listed in table below:

Table 5.1 Parameters Used During Friction Estimation

Parameter	Value	Unit
Piston Seal		
Hardness	70	$ShoreA$
O-Ring Compression	10%	-
fc_{piston}	0.7	-
fh_{piston}*	23	-
L_p	4.72	$inch$
A_p	0.26	$inch^2$
Rod Seal		
Hardness	90	$ShoreA$
O-Ring Compression	10%	-
fc_{rod}	1.6	-
fh_{rod}**	$75 - 70 - 30$	-
L_p	1.37	$inch$
A_p	0.9	$inch^2$

* fh_{piston} estimation is done according to $30bar$.

** fh_{rod} estimation is done according to $300bar - 200bar - 60bar$.

Using the parameters presented in Table 5.1, $F_{coul,piston}$ can be estimated as $41N$. $F_{coul,rod}$ is calculated as $30N - 28N - 12N$ for $300bar - 200bar - 60bar$ pressure levels. At intermediate pressure levels, $F_{fric,rod}$ is calculated by cubic interpolation.

B. Simulink Model

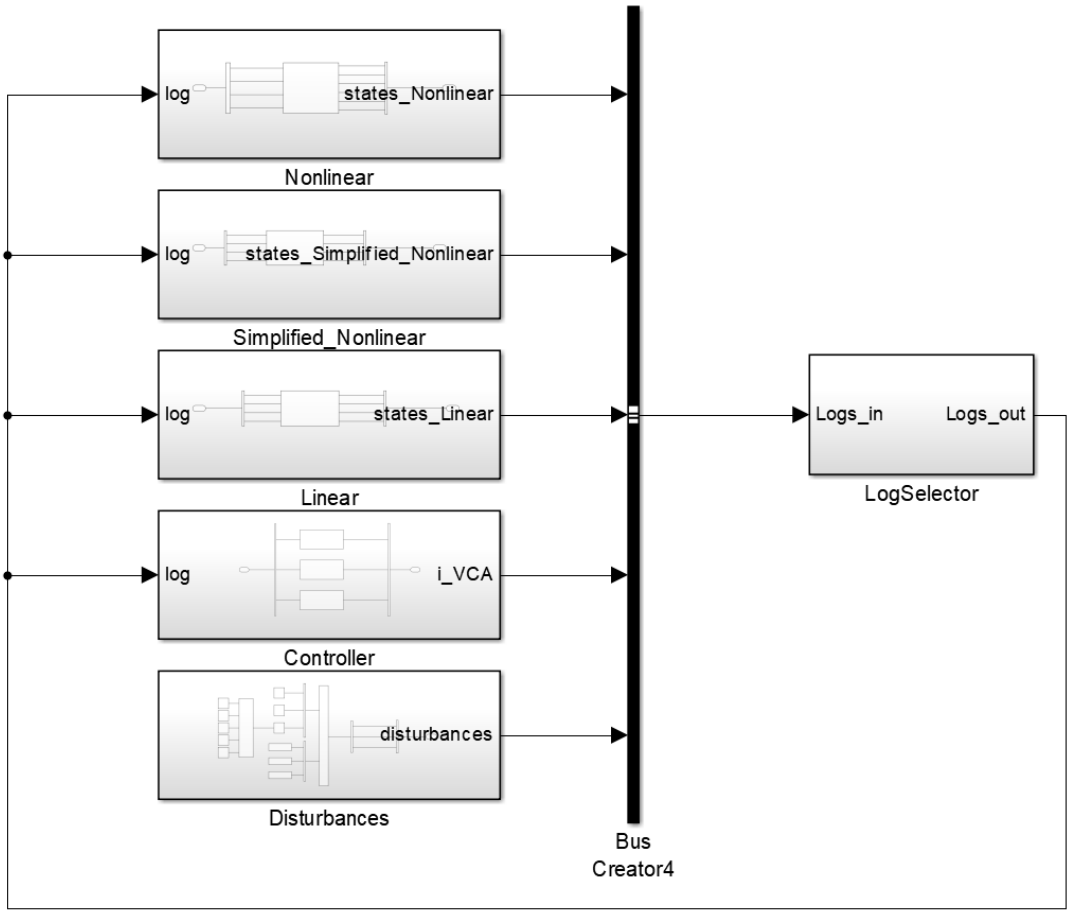

Figure 5.3. Main Simulation Model

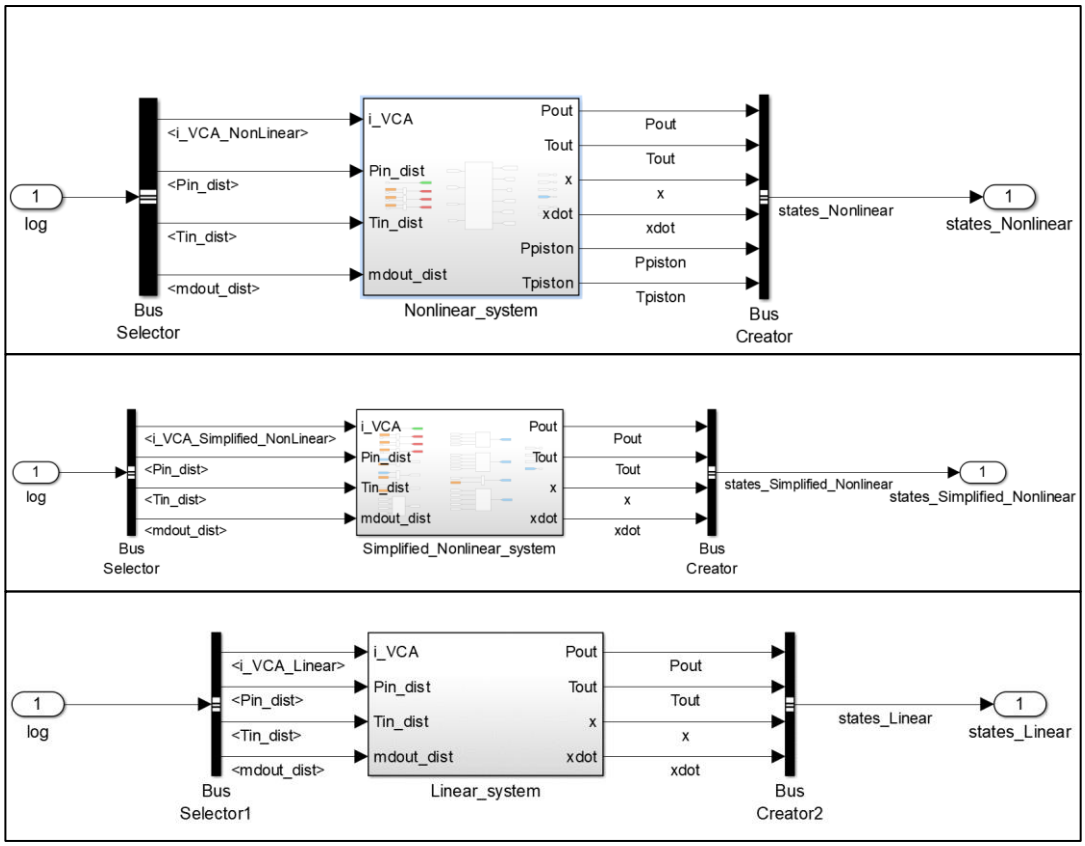

Figure 5.4. Nonliner, Simplified Nonlinear and Linear System Model Blocks

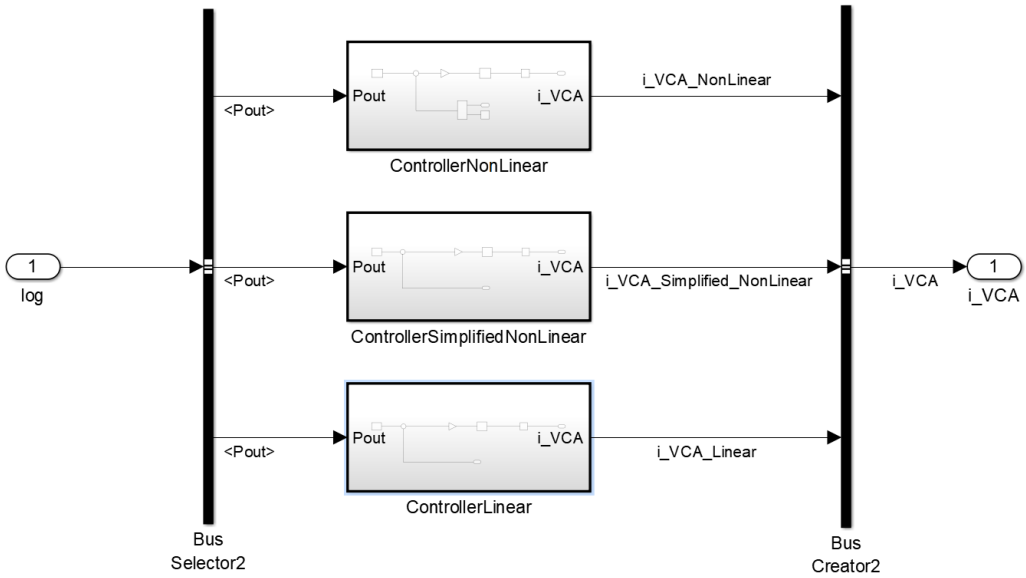

Figure 5.5. Controller Block

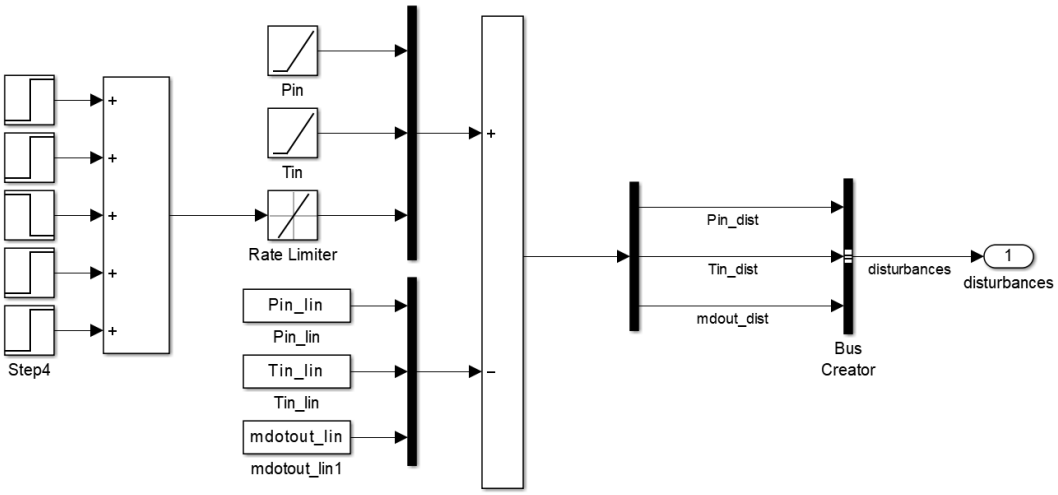

Figure 5.6. Disturbance Block